AD-A189 607 CONTROL OF STRUCTURE IN TURBULENT FLOWS: BIFURCATING AND BLOOMING JETS (U) STANFORD UNIV CA DEPT OF MECHANICAL ENGINEERING W C REYNOLDS ET AL 10 OCT 87 1/1

UNCLASSIFIED AFOSR-TR-88-0036 F49620-84-K-0005 F/G 20/4 NL

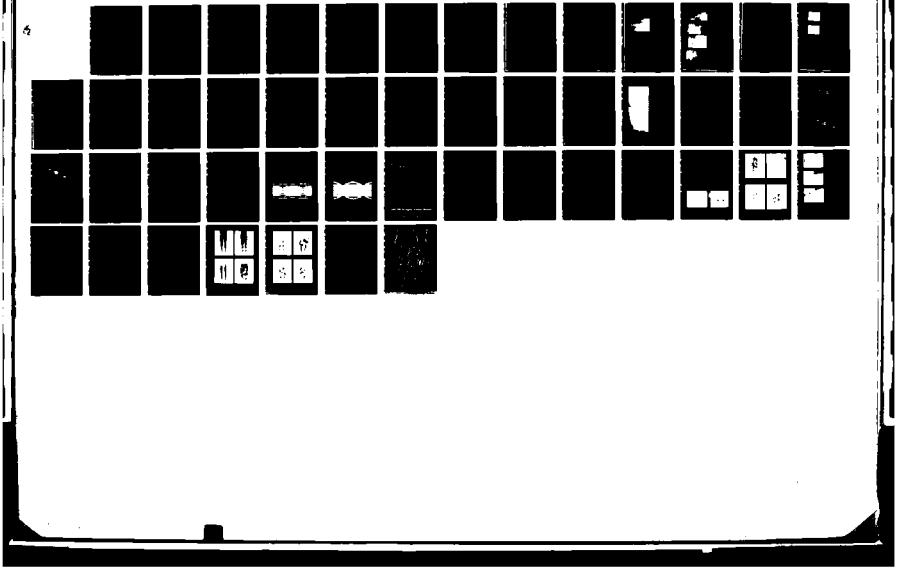

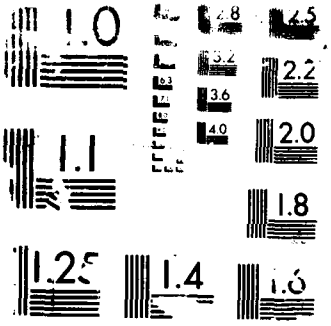
1.0
1.1
1.25
1.4
1.6
1.8
2.0
2.2

(2)

SECURITY

AD-A189 607 T DOCUMENTATION PAGE

1a REPOR UNCLASSIFIED	1b RESTRICTIVE MARKINGS
2a SECURITY CLASSIFICATION AUTHORITY	3 DISTRIBUTION / AVAILABILITY OF REPORT Approved for public release; distribution unlimited.
2b. DECLASSIFICATION / DOWNGRADING SCHEDULE	
4. PERFORMING ORGANIZATION REPORT NUMBER(S)	5. MONITORING ORGANIZATION REPORT NUMBER(S) AFOSR-TR- 88-0036
6a. NAME OF PERFORMING ORGANIZATION STANFORD UNIVERSITY	6b OFFICE SYMBOL (If applicable)
6c. ADDRESS (City, State, and ZIP Code) STANFORD, CA 94305	7a. NAME OF MONITORING ORGANIZATION AFOSR/NA
	7b ADDRESS (City, State, and ZIP Code) BUILDING 410 BOLLING AFB, DC 20332-6448
8a. NAME OF FUNDING SPONSORING ORGANIZATION AFOSR	8b OFFICE SYMBOL (If applicable) NA
8c. ADDRESS (City, State, and ZIP Code) BUILDING 410 BOLLING AFB, DC 20332-6448	9 PROCUREMENT INSTRUMENT IDENTIFICATION NUMBER AFOSR 84-K-0005 F49620
	10 SOURCE OF FUNDING NUMBERS PROGRAM ELEMENT NO: 61102F; PROJECT NO: 2307; TASK NO: A2; WORK UNIT ACCESSION NO:

11 TITLE (Include Security Classification)
CONTROL OF STRUCTURES IN TURBULENT FLOWS; BIFURCATING AND BLOOMING JETS

12 PERSONAL AUTHOR(S)
W. C. REYNOLDS AND D. E. PAREKH

13a TYPE OF REPORT	13b. TIME COVERED	14. DATE OF REPORT (Year, Month, Day)	15. PAGE COUNT
FINAL	FROM 2/1/84 TO 5/31/87	87/10/10	45

16 SUPPLEMENTARY NOTATION

17 COSATI CODES		
FIELD	GROUP	SUB-GROUP

18. SUBJECT TERMS (Continue on reverse if necessary and identify by block number)
JETS; FLOW CONTROL; TURBULENCE STRUCTURE

19 ABSTRACT (Continue on reverse if necessary and identify by block number)
The combinatin of properly-selected axial and orbital excitation has been shown to have dramatic effect on the structure and mixing of round jets. Experiments and numerical simulations show that these phenomena are due to interaction between the large-scale vortices in the jet near field. The position and phasing of these vortices can be altered by relatively weak excitation, causing the jet to divide into two separate jets (bifurcation) or to explode (bloom) in a shower of vortex rings. This report summarizes the key results of studies in water and low-speed air flows.

20 DISTRIBUTION / AVAILABILITY OF ABSTRACT ☒ UNCLASSIFIED/UNLIMITED ☐ SAME AS RPT ☐ DTIC USERS	21 ABSTRACT SECURITY CLASSIFICATION UNCLASSIFIED
22a NAME OF RESPONSIBLE INDIVIDUAL JAMES MCMICHAEL	22b. TELEPHONE (Include Area Code) 202-767-4936 / 22c. OFFICE SYMBOL NA

DD FORM 1473, 84 MAR 83 APR edition may be used until exhausted
All other editions are obsolete.

SECURITY CLASSIFICATION OF THIS PAGE
UNCLASSIFIED

CONTROL OF STRUCTURE IN TURBULENT FLOWS: BIFURCATING AND BLOOMING JETS

by

W. C. Reynolds and D. E. Parekh

FINAL REPORT

Prepared from work done under Contract

AF-F49620-84-K-0005

Thermosciences Division
Department of Mechanical Engineering
Stanford University
Stanford, California 94305

October 1987

Executive Summary

1. Objectives

Techniques for controlling the behavior of turbulent fluid flows are beginning to be developed as a result of fundamental understanding of the basic mechanisms active in turbulent flows. For example, by properly combining axial and helical (orbital) disturbances, one can cause a round turbulent jet to split into two distinct jets (*bifurcating jets*) or to explode into a shower of vortex rings forming a rapidly-mixing, wide-angle conical spreading flow (*blooming jets*). These phenomena were discovered in an NSF-funded program under the Principal Investigator, which led to extensive research on dual-mode forcing under AFOSR support. This report summarizes the research accomplished under AF-F49620-84-K-0005.

The general objective of this work is to control jet flows by properly organizing the dominant large-scale vortex structures. The work has focused on understanding the influence of excitation frequency and amplitude on the large-scale structures of these flows at various Reynolds numbers. Specifically, the effects of dual-mode forcing on the structure, momentum, and mixing characteristics of turbulent jets have been investigated using a combination of laboratory experiments and numerical simulations.

2. Overview of results

Dramatic changes in jet development described above were discovered by Lee and Reynolds (1985a; see Appendix A) in a study of mechanically-excited water jets at a Reynolds number of 4,000. The axial excitation was provided by weak pulsations in the jet flow and the orbital excitation by mechanical motion of the nozzle. The basic flow regimes and flow structure were determined using flow visualization with dye and laser-induced-fluorescence. A fiber-optic laser-doppler-anemometry system was used to measure the velocity field and momentum mixing, and acid-suppressed laser-induced fluorescence was used to study molecular mixing. This work is reported in detail by Lee and Reynolds (1985b).

To provide insights into the governing mechanisms and to study the effect of various parameters, a vortex-filament code for simulating the large-scale characteristics of excited jets was developed in cooperation with NASA/Ames (Leonard, Couet, and Parekh 1985; see Appendix B). This work provided confirmation of the mechanism of bifurcation and blooming. Concentric vortex rings, the dominant flow structures in the near field of a normal jet, leapfrog over one another axisymmetrically. These rings are made eccentric from one another by orbital excitation, and eccentric rings tend to tilt one another. Under the right conditions, this interaction forces them apart. In dual-mode excitation, the axial excitation controls the phasing of the vortex rings, and the orbital excitation controls the azimuthal phasing of the rings. If two rings are shed per orbit, and the spacing between them is in a certain range, the jet will bifurcate. If the frequency ratio is a fraction in a certain range, the jet will bloom into a shower of independent vortex rings.

While on sabbatical leave at Caltech in 1984, the Principal Investigator constructed a second water apparatus in which bifurcation and blooming were demonstrated with a smaller diameter jet that allowed visualization up to 100 diameters downstream. There it was shown that the bifurcation is permanent, and hence the far field of a bifurcating jet is dramatically different than that for a normal jet with the same momentum flux.

The experimental results in the water facility and the numerical simulation suggested that similar control of jet flows could be achieved in air jets at higher Reynolds numbers. The challenge at high Reynolds numbers is to force "collective interactions" of the closely-spaced vortices in the thin shear layer occurring at high Reynolds number, so that the spacing of the resulting large vortices is placed in the range necessary for bifurcation or blooming. A simple air flow apparatus was constructed in which it was found that weak acoustic excitations not requiring mechanical nozzle motion would produce the bifurcating/blooming phenomena at Reynolds numbers up to 20,000. (Parekh, Reynolds, and Mungal 1987; Appendix C). Subsequently another air apparatus for higher-speed experimentation was constructed, and it was found that the phenomena could be produced by acoustic excitation at a Reynolds number of 100,000, M = 0.22, where the vortex rings undergo transition to turbulence before the bifurcation or blooming (Parekh and Reynolds 1987; Appendix D). This provided the first clear evidence that the phenomena could be effected in flows of primary technical interest to the AFOSR.

3. Summary of principal conclusions

1. Properly combined axial and helical excitations can produce significant changes in the evolution of round turbulent jets, including spreading angles as large as 80 degrees.
2. Bifurcating and blooming jets are dominated by vortex rings which evolve in well-defined patterns governed by the ratio of axial-to-helical excitation frequencies.
3. Bifurcating jets occur when the axial/orbital frequency ratio is 2 and the axial Strouhal number is between 0.3 and 0.7. Within this range, the spreading angle increases with axial Strouhal number.
4. *The two branches of the bifurcating jet evolve as separate jets, apparently* indefinitely far from the jet exit.
5. Blooming jets occur when the axial/orbital frequency ratio is non-integer between 1.7 and 2.8 and the axial Strouhal number is between 0.3 and 0.7. Within this range, the spreading angle increases with axial Strouhal number.
6. Molecular mixing is enhanced in blooming jets.
7. Increasing either the axial or helical excitation amplitude can cause the spreading angle of the bifurcating jet to increase. However, increasing amplitudes too high results in saturation that inhibits further increases in spreading angle.
8. One can model the governing mechanism in these flows as a vortex-interaction process.
9. Acoustic excitations can be used to force bifurcation or blooming in air jets at Reynolds numbers up to at least 100,000 and Mach numbers up to 0.22. With sufficient power in the forcing, the phenomena can probably be effected at any Reynolds number and subsonic Mach number.

4. Future plans

Additional experiments in the high-speed air facility are needed to establish the excitation amplitudes required for bifurcation and blooming flow control of high Reynolds number jets at moderate Mach Numbers. This is now being accomplished under other AFOSR funding.

Methods for use of the flow power to produce the required oscillation need to be developed if the phenomena are to be produced in large jets at high speeds. Methods for accomplishing this are now being explored under other AFOSR funding.

References, presentations, and publications

Lee, Mario and W. C. Reynolds 1983, "Structure of the Bifurcating Jet," *Bulletin of the American Physical Society*, vol. 28, no. 9, p. 1362.

Lee, Mario, and W. C. Reynolds 1985a, "Bifurcating and Blooming Jets," *Fifth Symposium on Turbulent Shear Flows*, Ithaca, New York, pp. 1.7-1.12.

Lee, Mario, and W. C. Reynolds 1985b, "Bifurcating and Blooming Jets," Report TF-22, Thermosciences Division, Department of Mechanical Engineering, Stanford University.

Leonard, A., B. Couet, and D. Parekh 1985, "Two Studies in Three-Dimensional Vortex Dynamics: A Perturbed Round Jet and an Inhomogeneous Mixing Layer," *International Symposium on Separated Flow*, Trondheim, Norway.

Parekh, D. E., A. Leonard, and W. C. Reynolds 1983, "A Vortex-Filament Simulation of a Bifurcating Jet," *Bulletin of the American Physical Society*, vol. 28, no. 9, p. 1353.

Parekh, D. E., W. C. Reynolds, and M. G. Mungal 1986, "Bifurcating Air Jets," *Bulletin of the American Physical Society*, vol. 31.

Parekh, D. E., W. C. Reynolds, and M. G. Mungal 1987, "Bifurcation of Round Air Jets by Dual-Mode Acoustic Excitation," AIAA paper 87-0164, presented at AIAA 25th Aerospace Sciences Meeting, Reno, Nevada.

Parekh, D. E., and W. C. Reynolds 1987, "Bifurcating Air Jets at Higher Subsonic Speeds," *Sixth Symposium on Turbulent Shear Flows*, Toulouse, France.

Participants

Principal Investigator:

W. C. Reynolds, Professor, Mechanical Engineering, Stanford

Collaborating Investigators:

M. G. Mungal, Assistant Professor, Mechanical Engineering, Stanford
A. Leonard, previously: Research Scientist, NASA Ames Research Center
currently: Professor, California Institute of Technology

Research Assistants:

M. J. Lee, doctoral graduate, 1985, Mechanical Engineering, Stanford
D. E. Parekh, doctoral candidate, 1988, Mechanical Engineering, Stanford
P. Juvet, doctoral candidate, 1991, Mechanical Engineering, Stanford

Bifurcating and Blooming Jets

M. J. Lee and W. C. Reynolds
Stanford University
Stanford, CA

FIFTH SYMPOSIUM
ON TURBULENT SHEAR FLOWS
Ithaca, New York
1985

BIFURCATING AND BLOOMING JETS

Mario Lee and W. C. Reynolds
Department of Mechanical Engineering
Stanford University, CA 94305

ABSTRACT

This paper is concerned with the control of a round jet discharging into quiescent fluid. The fluid is water, and the jet is excited by a combination of axial and orbital excitations. The axial excitations are introduced through motion of a diaphragm on the piston that drives the main flow, and the orbital excitations are produced by orbital motion of the tip of the nozzle. The Reynolds number based on diameter and exit velocity is 4300. Some surprising results are obtained when the ratio (R) of the axial frequency to the orbital frequency is in the range of 1-4. When R = 2, the jet bifurcates into two separate ring-vortex trains, and when R = 3, the jet divides into three jets in an equilateral array. When R is non-integer in the range of 1.6-3.2, the jet "blooms" and fills a cone of 80° included angle with vortex rings. This produces a very rapid spreading of the jet. Velocity measurements made at 6.5 and 8 diameters away from the nozzle show a double-peak profile for the bifurcating and blooming jets. These results show that large changes can be produced in round jets under controlled excitation.

NOMENCLATURE

A_o	Orbital excitation amplitude. Peak to peak displacement of the nozzle lip.
D	Diameter of the nozzle.
f_a	Axial excitation frequency, Hz.
f_o	Orbital excitation frequency, Hz.
R	Ratio of axial-to-orbital excitation frequency, f_a/f_o.
Re	Reynolds number based on the average jet velocity U_{ave} and jet diameter, $U_{ave}D/\nu$.
r	Radial axis away from the jet centerline in a cylindrical coordinate system.
St_a	Axial Strouhal number based on diameter and average jet velocity, f_aD/U_{ave}.
St_o	Orbital Strouhal number based on diameter and average jet velocity, f_oD/U_{ave}.
U	Mean axial velocity.
U_{ave}	Average jet velocity based on jet diameter and the volume discharge rate from the nozzle.
U_o	Mean centerline velocity of the natural jet measured at 0.15 diameters away from the nozzle.
u'	Root-mean-square value of the axial velocity.
x	Streamwise direction along the centerline of the jet in a cylindrical coordinate system.
θ	Azimuthal angle.
ν	Kinematic viscosity.

INTRODUCTION

Numerous studies in the past have tried to control the evolution of round, turbulent jets using controlled excitation. Sarohia and Bernal [1] attempted to improve mixing by pulsing the mean flow of a round turbulent jet. Viets [2] advocated the use of oscillating jets and developed a fluidic actuator. Perry and Lim [3] obtained long, coherent, vortical structures while exciting a coflowing jet with lateral oscillations. The present study was inspired by Binder and Favre-Marinet [4], who showed that the effects of flapping a two-dimensional jet are felt far away from the nozzle. This led to the idea of controlling the evolution of jets through combined axial and orbital excitation.

Therefore, the objective of this investigation was to study the near-field response of a round jet under varying combinations of axial and orbital excitation frequencies. The results were documented with the aid of flow visualization using dye injection.

Velocity profiles at various downstream locations were measured with a Laser-Doppler anemometry system having an optical-fiber link between the laser and the transmitting optics.

EXPERIMENTAL FACILITY

The facility consisted of a large piston-and-cylinder arrangement as shown in Fig. 1. The jet was formed by pushing water out of a 1/2-inch-diameter (D) nozzle which exited into the bottom of a square plexiglas tank. The piston was activated after the water was at rest and free of any motion. Sinusoidal perturbations were imposed on the mean flow through motion of a flexible diaphragm situated on top of the piston. The diaphragm was set into motion by a hydraulic system and driven by a motor through a set of compound levers and cams. The details of this system have been described by Bouchard [5].

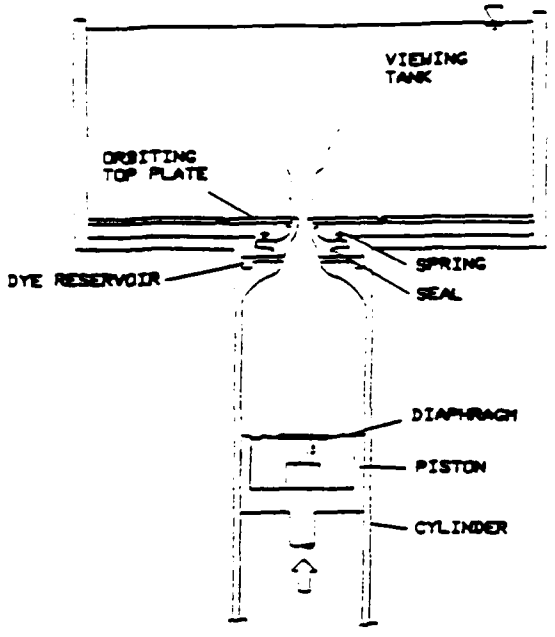

EXPERIMENTAL APPARATUS

Fig. 1. Schematic of experimental facility.

The orbital excitation was achieved by moving the tip of the nozzle in an orbital fashion through a drive plate and four equally spaced push-rods. As shown in Fig. 2, the peak-to-peak motion (A_o) of the tip of the nozzle was approximately 0.018 inches. The spring-loaded nozzle thus precessed about the system axis at an angle of 0.2°.

EXPERIMENTAL METHOD

To visualize the structure in the flow, diluted food coloring was injected circumferentially through the dye slots shown in Fig. 2. The dye injected into the boundary layer of the nozzle marks the shear layer as it developed. Both 35 mm snapshots and 16 mm cine film were made of the flows.

A single-component, laser-Doppler anemometry system in the forward-scatter mode was employed to

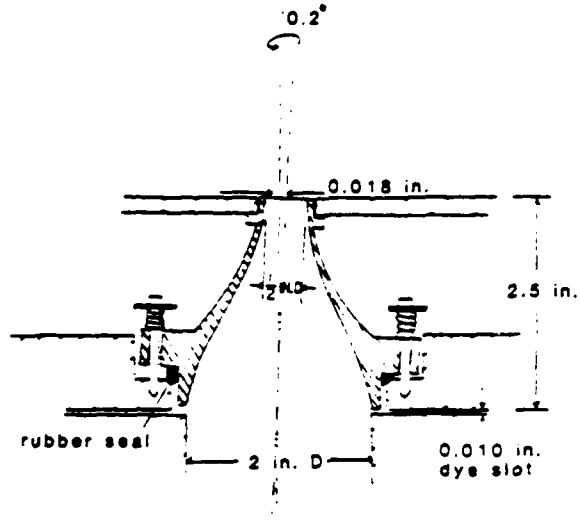

Orbital Motion of Nozzle
(not to scale)

Fig. 2. Orbital motion of nozzle.

measure the streamwise component of velocity. Green laser light was guided to the transmitting optics (TSI, Inc.) through a polarization-preserving, single-mode optical fiber (NRC model P-SPV-10) as shown in Fig. 3. The optical fiber allowed flexibility in alignment and traverse of the measuring volume. The effective measuring volume was 0.3 mm wide and 2 mm long. Although many systems have been designed and proposed based on optical fibers, the system configuration follows that of Meakin et al. [6] for simplicity. The details of this system and the orbital excitation mechanism have been described previously [7].

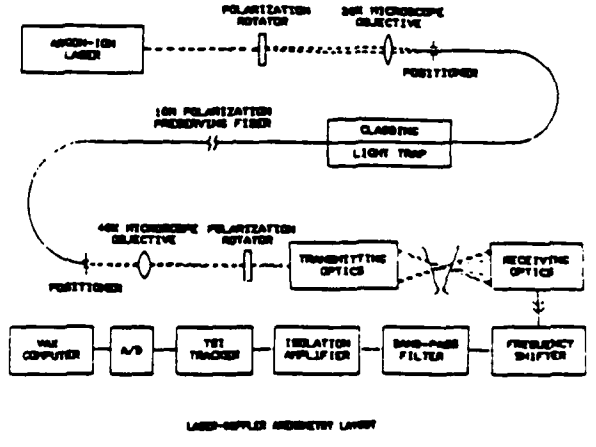

Fig. 3. Schematic of laser-Doppler anemometry system.

NATURAL JET

At a Reynolds number of 4300, the observed near field structure of the natural jet without artificial excitation is consistent with the observations of Browand and Laufer [8] and Bouchard [5]. A snapshot of the natural jet using dye injection can be found in

Fig. 4. Close to the nozzle, the shear layer separates from the lip and rolls up into vortex rings. The formation of the rings is irregular in time. In the present flow, the average shedding rate was 26 Hz, based on 16 mm movies. The ring vortices underwent interaction in which the downstream ring would grow and slow down while the following ring increased in speed as it shrank in size. The upstream ring then passed through the center of the ring in front and finally coalesced together to form a single ring. At about five diameters, the rings broke down into three-dimensional puffs as the jet turned turbulent.

Fig. 4. Natural jet at Re = 4300.

Velocity measurements of the natural jet taken at 0.15 diameters downstream (x/D = 0.15) showed that the mean velocity was flat within 1.5% (Fig. 5). The average jet exit velocity (U_{ave}) was 0.307 m/s, and the centerline velocity (U_o) was 0.327 m/s. The shear layer had a half-slope thickness of 0.07 diameters with a centerline fluctuation (u') of less than 1% at x/D = 0.15. Velocity profiles of the natural jet up to eight diameters downstream appear symmetric, with a smooth, bell-shaped curve.

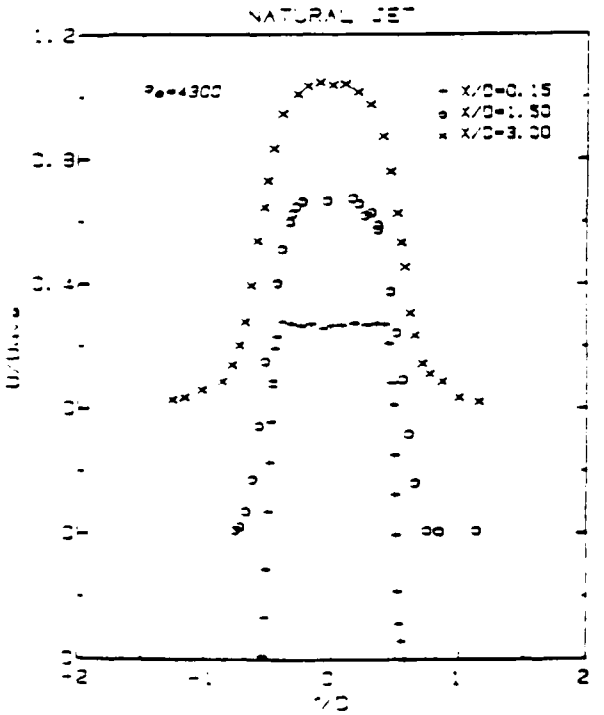

Fig. 5. Velocity profiles of natural jet.

EFFECTS OF COMBINED AXIAL AND ORBITAL EXCITATION

In the present study, a sinusoidal pertubation of 17% was imposed on the mean flow. The axial jet responded to the imposed excitation by shedding vortex rings at the excitation frequency. Visualization showed that all vortex-ring coalescence was suppressed by this excitation.

When the axial and the orbital excitations were both imposed on the jet, dramatic changes were observed. The dimensionless number R defined as the ratio of axial-to-orbital excitation frequency is an important parameter characterizing the flows. An interesting overview of the various types of jets can be obtained when the axial excitation frequency (f_a) is fixed at 12 Hz while increasing the orbital excitation frequency (f_o) as R decreases, where Re = 4300. This will now be reviewed.

At low orbital frequencies, the global features of the flow are similar to those of an axially excited jet. Vortex rings are observed to shed regularly at the axial excitation frequency of 12 Hz. In addition, the vortex-ring train exhibits a slightly sinuous behavior.

When the orbital frequency is gradually increased, the vortex rings begin to tilt and collide with each other, breaking up at about five diameters from the nozzle. During this process, the dye which marks the shear layer is observed to disperse at a larger angle when compared with a natural jet. The observed dispersion angle is about 40° when R = 4. When R is further decreased to a value between 3 and 4, vortex rings intermittently move away from the jet axis at an angle. The vortex rings that move away from the jet axis remain coherent for five to ten diameters.

When the value of R is approximately 3, the jet splits up into three branches with a slight precession. The precession disappears when R = 3, with the jet forming an equilateral array. Because of this flow pattern, the flow is called a "trifurcating" jet. A similar phenomenon can be observed when R = 2 (Fig. 6). In this case, the jet bifurcates into a Y-shaped pattern in opposite directions. Figure 7 shows an on-axis view of the "bifurcating" jet issuing out of the plane where R = 1.9. The precession of the bifurcating jet is indicated by two spiraling trails of dye deposited by the vortex rings as they break up. Occasionally, a secondary forking of one of the branches can be seen. This type of jet is called a "bifurcating" jet because of the unique forking behavior of the vortex rings. The angle between the axes of the two branch of vortex rings has been observed to be as large as 90°.

At R = 1.7, vortex rings can be seen flying away from the centerline along a side of a cone in all directions. A picture of this phenomenon is shown in Fig. 8. The flow field resembles that of a flower blooming when viewed on axis (Fig. 9), and hence the flow is called a "blooming" jet. This phenomenon persists for a range of R = 3.2-1.6.

When the orbital excitation frequency is further increased such that R falls below 1.6, the dispersion angle of the vortex rings drastically decreases. At R < 1.3, the vortex rings break up very early during the roll-up.

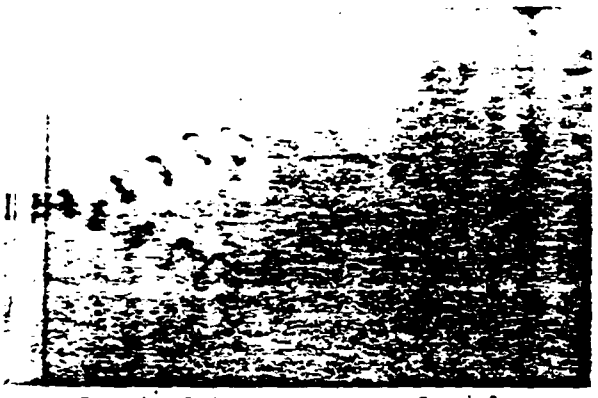

Fig. 6. Bifurcating jet at R = 1.9.

Fig. 7. End view of bifurcating jet.

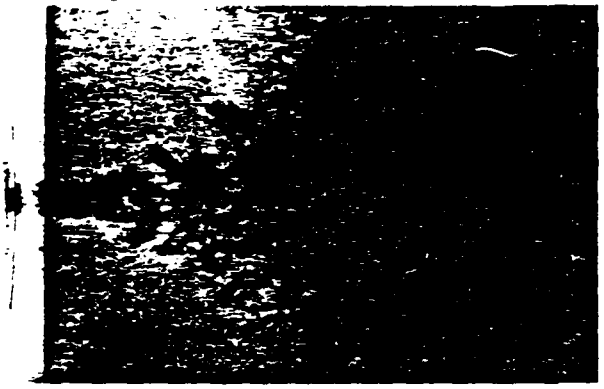

Fig. 8. Blooming jet at R = 1.7.

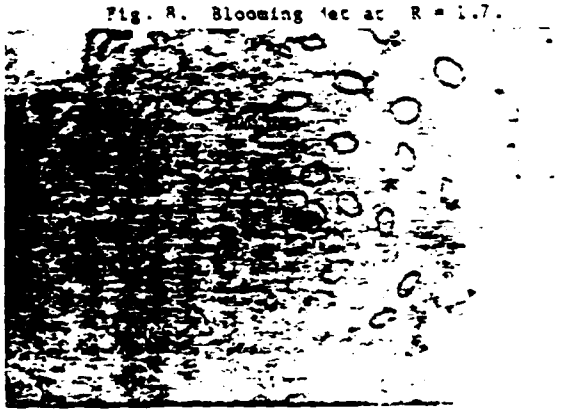

Fig. 9. End view of blooming jet.

CLASSIFICATION OF FLOW FIELD

In an attempt to map out the different types of jets, dye injection was used to visualize various flows at Reynolds numbers of 2800, 4000, 5500, 8300 and 10,000. Some of the jets are marked on the parameter plot shown in Fig. 10. The frequencies are normalized by D and U_{ave} to form axial (St_a) and orbital (St_o) Strouhal numbers. The open symbols represent excited jets whose vortex rings have been observed to break up before being able to propagate away from the centerline. The closed symbols represent excited jets whose vortex rings remain coherent more than two diameters away from the centerline. Within the region roughly marked by the closed symbols, bifurcating, trifurcating, and blooming jets can be found. For simplicity, the area is called the "blooming" region. The region lies roughly between R = 1.6-3.2. Furthermore, the region is confined between St_a = 0.35-0.75 and St_o = 0.15-0.35. When R = 2, the jet bifurcated into a Y-shaped pattern, and when R = 3, the jet splits up into three branches. If the value of R ≈ 2 or 3, the jet is observed to precess with the corresponding flow patterns. When R takes on non-integer values within the region, the jets "bloom" to fill a cone of 30° included angle.

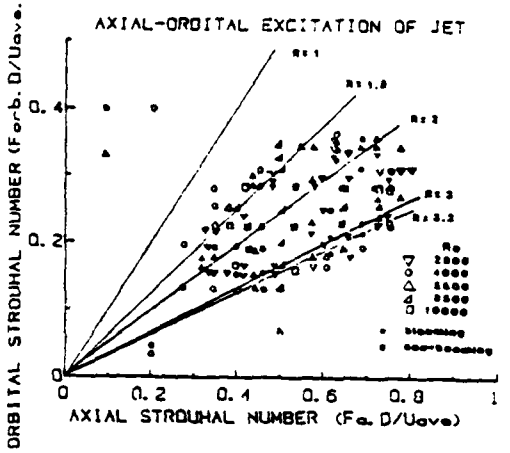

Fig. 10. Parameter plot of bifurcating and blooming jets.

FLOW STRUCTURES

Based on the dye-injection photographs, the appearance of the excited jets is very different from that of the natural jet. Besides the tremendous increase in the spreading angle, a bifurcating jet loses its axisymmetry and exhibits two planes of symmetry. The first plane of symmetry lies along a diametric plane containing the two branches of the jet called the plane of bifurcation. The second plane of symmetry bisects the two branches and is called the bisecting plane. In the case of the blooming jet, the axisymmetry appears to be retained.

Within these complicated flow fields, the following fluid motion can be deduced. Figure 11 shows a schematic of a bifurcating jet in which the solid line marks the boundary between the jet and ambient fluid. In the first few diameters, layers of jet and ambient fluid roll up to form vortex rings. Downstream of the fork in the flow, the jet fluid must be stretched back and forth between two branches because of the alternating motion of successive rings. In the same fashion, blooming jets would exhibit a similar motion in

which the jet fluid is stretched back and forth in all azimuthal directions.

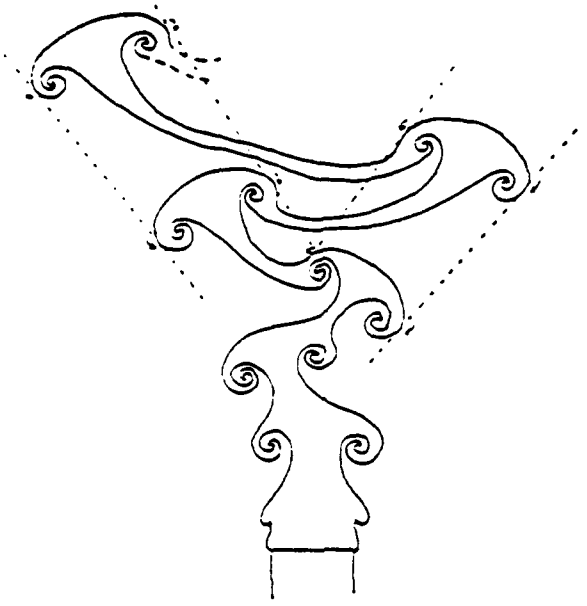

Fig. 11. Schematic of a bifurcating jet with trajectories of induced downwash.

VELOCITY PROFILES

Mean-velocity profiles measured at various downstream locations of the blooming jet (R = 2.4) and in the plane of bifurcation of the bifurcating jet (R = 2) reveal some interesting developments. The Reynolds number is 4300 and f_a = 12 Hz. In the first three diameters, both bifurcating and blooming jets exhibit a flat top-hat-shaped profile which gradually smoothes out into a bell-shaped curve like a natural jet. From four to eight diameters downstream, a double-peak profile develops in both bifurcating (Fig. 12) and blooming (Fig. 13) jets. These peaks appear to coincide with the location of the coherent vortex rings which split up and move away from the jet centerline. Since the vortex rings are probably the most energetic structures in these flows, this observation is expected. What is surprising are the additional dips within the double-peak profiles of the bifurcating jet at 6.5 and 8 diameters. The double peaks of the blooming jet develop at about the same location but without the additional dips.

In an attempt to understand the origin of the dips, velocity-time traces for one second at x/D = 6.5 were recorded on an oscilloscope at locations inside the dip and at the peaks of the bifurcating jet. Figure 14 shows a comparison between the two traces. Although both traces reveal a regular fluctuation of 6 Hz (vortex-passing frequency) and about the same peak velocity, the bottom trace recorded in the dip shows much lower valleys. If the schematic of a bifurcating jet is analyzed, as shown in Figure 11, four trajectories can be seen along which a large downwash component of velocity is induced by the repeated passing of vortex rings. The repeated passage of the vortex rings in this location could lead to the formation of the dips in the velocity profiles as observed. In the blooming jet, dips do not appear because the rings do not follow each other along fixed trajectories as in a bifurcating jet. Therefore, the downwash component of velocity induced by each vortex ring is not reflected in the time-averaged velocity profiles.

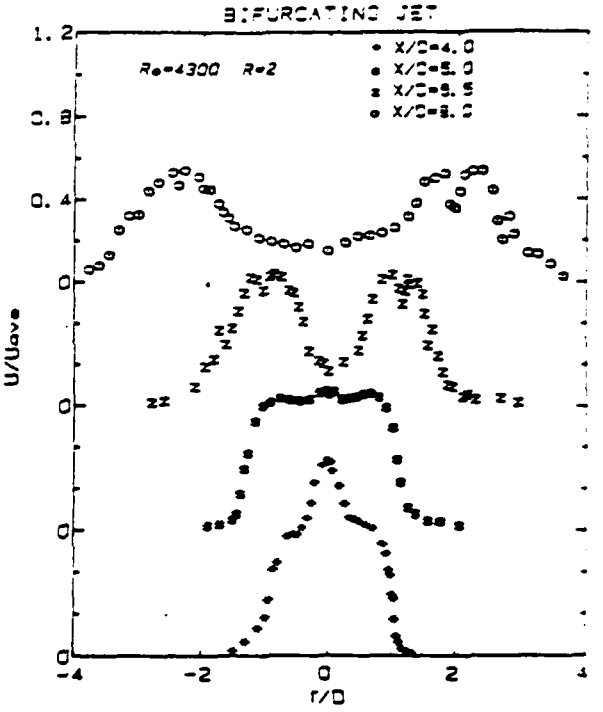

Fig. 12. Mean-velocity profiles of bifurcating jet.

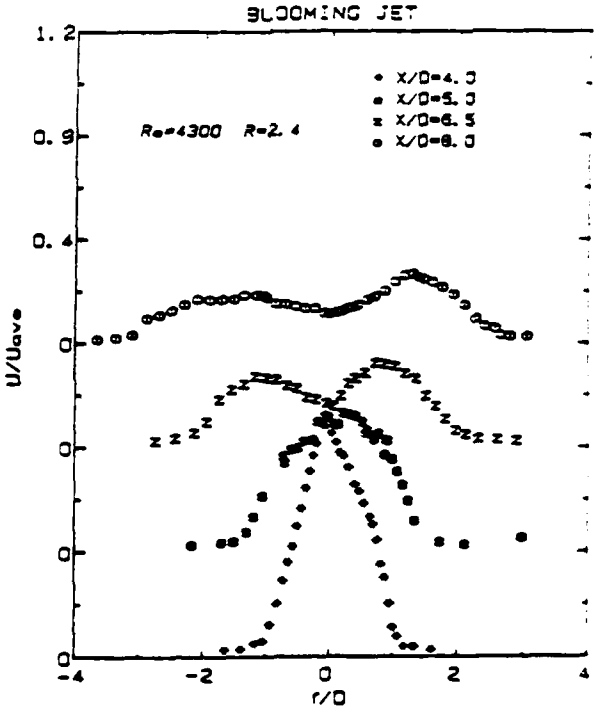

Fig. 13. Mean-velocity profiles of blooming jet.

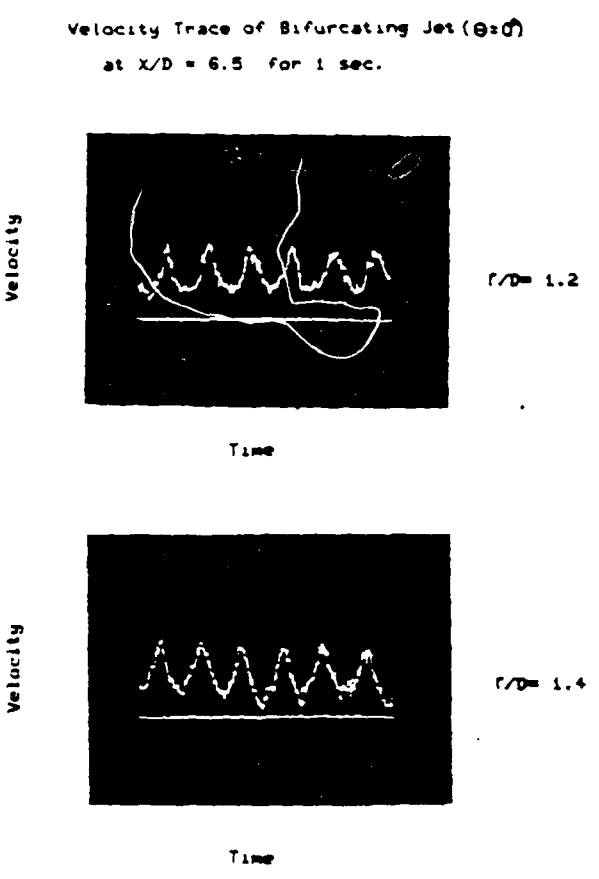

Fig. 14. Velocity traces of a bifurcating jet.

CONCLUSIONS

In summary, the spreading angle of a round jet has been tremendously increased by imposing axial and orbital excitation on the flow. The axial excitations are small pulsations of the mean flow, and the orbital excitations are small orbital motions of the lip of the nozzle. Different flow fields called bifurcating and blooming jets have been observed. A bifurcating jet consists of vortex rings split up into two trains in a V-shaped pattern and is produced when the axial excitation frequency is two times that of the orbital. When the ratio of excitation frequencies takes on non-integer values, the jet "blooms" to fill a cone of 80° included angle with vortex rings moving along the side. Observations based on dye injection and velocity measurements show that controlled axial and orbital excitation can produce a large change in the development of round, turbulent jets.

ACKNOWLEDGMENT

The authors gratefully acknowledge the financial support of the Air Force Office of Scientific Research (AF-F49620-84-K-0005).

REFERENCES

1. Sarohia, V., and Bernal, L. P., "Entrainment and Mixing in Plusatile Jets," Proc. 3rd Symp. Turb. Shear Flow, 11.30-11.35, (1981).

2. Viets, H., "Flip-Flop Jet Nozzle," A.I.A.A. Journal, 13: 1375-1379, (1975).

3. Perry, A. E., and Lim, T. T., "Coherent Structures in Coflowing Jets and Wakes," J. Fluid Mech., 88: 451-463, (1978).

4. Binder, G., and Favre-Marinet, "Some Characteristics of Pulsating or Flapping Jets," Unsteady Turbulent Shear Flows, Symposium of the International Union of Theoretical and Applied Mechanics, Toulouse, France. Springer-Verlag. pp. 370-379, (1981).

5. Bouchard, E. E., and Reynolds, W. C., "The Effects of Forcing on the Mixing-Layer Region of a Round Jet," Unsteady Turbulent Shear Flows, Symposium of the International Union of Theoretical and Applied Mechanics, Toulouse, France, Springer-Verlag, pp. 402-411, (1981).

6. Meakin, R. L., Koseff, J. R. and Street, R. L., "A Fiber Optical Link for Modular Two Component LDA Optics and Argon-ion Laser," Proceedings of the 2nd International Symposium on Applied Laser Anemometry to Fluid Mechanics, Lisbon, Portugal, (1984).

7. Mario Lee, "Bifurcating and Blooming Jets," Ph.D. dissertation, Mech, Eng. Dept., Stanford University, Stanford, California (1985).

8. Browand, F. K., and Laufer, J., "The Role of Large Scale Structures in the Initial Development of Circular Jets," Proc. 4th Symposium on Turbulence in Liquids, Univ. Missouri-Rolla (1975).

TWO STUDIES IN THREE-DIMENSIONAL VORTEX DYNAMICS: A PERTURBED ROUND JET AND AN INHOMOGENEOUS MIXING LAYER

Author: Anthony Leonard
Benoit Couët
David Parekh

Date: April 23, 1985

Project: FMN003

ABSTRACT

Three-dimensional vortex simulations are used to study the remarkable structure of the round jet with imposed axial and orbital excitations and to investigate the dynamics of an inhomogeneous mixing layer in which the unperturbed state is an infinite array of Stuart vortices. The simulations reveal the nonlinear vortex interactions of importance that control the structure and development of these flows.

Invited lecture, International Symposium on Separated Flow around Marine Structures, Trondheim, Norway, June 26-28, 1985.

TWO STUDIES IN THREE-DIMENSIONAL VORTEX DYNAMICS: A PERTURBED ROUND JET AND AN INHOMOGENEOUS MIXING LAYER

Anthony Leonard	NASA Ames Research Center	California, U.S.A.
Benoit Couët	Schlumberger-Doll Research	Connecticut, U.S.A.
David E. Parekh	Stanford University	California, U.S.A.

Abstract

Three-dimensional vortex simulations are used to study the remarkable structure of the round jet with imposed axial and orbital excitations and to investigate the dynamics of an inhomogeneous mixing layer in which the unperturbed state is an infinite array of Stuart vortices. The simulations reveal the importance of the nonlinear vortex interactions that control the structure and development of these flows.

1. INTRODUCTION

In this paper we discuss the computer simulation of complex three-dimensional fluid flows by vortex methods and give two applications. By simulation we mean that a large range of the important scales of motion in space and time are computed directly, as in large-eddy simulations. The flows we consider are at constant density and have high Reynolds numbers.

In a three-dimensional vortex method, vector elements of vorticity move at or near the local fluid velocity with the vectors strained by the local velocity gradient. These elements are required only where the vorticity is nonzero and are created only (1) to represent initial fields of vorticity or vorticity injected through computational boundaries, (2) to satisfy no-slip boundary conditions or (3) during "grid" refinement when one element may be split into two or more.

In many applications, the vorticity field is well represented by isolated, thin tubes. If the tubes are assumed to have zero cross section, a logarithmic divergence in the induced velocity is encountered. Thus the finite size of the vortex core must be taken into account in developing equations for vortex tube dynamics. As a result of such analyses, accurate equations for the long-wavelength dynamics of thin vortex tubes are available and form the basis for a three-dimensional vortex method, as discussed in Section 2. To discretize the vortex tubes, the space curve of each tube or filament is marked with a sequence of node points. Velocities of all the N nodes on the vortex filaments are computed from the infinite

medium Green's function (Biot-Savart law), requiring $O(N^2)$ operations per time step. The strain on the vortex elements, which, roughly speaking, are the vectors connecting adjacent nodes points on each filament, is accounted for automatically by the method.

In Section 3 we discuss the simulation of the excited round jet, using the thin-filament approximation. In this application, it had been observed experimentally that dramatic changes in the structure of the jet fluid are achieved by introducing axial and orbital excitations [6]. The interplay between computation and ongoing laboratory experiments has led to a basic understanding of the mechanisms that govern the structure of the jet and how they might be controlled.

In other applications, the vorticity field is a relatively smooth continuum. In this situation, vortex elements must be densely packed to represent properly the dynamics of the continuum. Recent mathematical proofs have shown that, when properly constructed, vortex methods will produce solutions that converge to the solution of the Euler equations as the number of computational elements increases [1,2,5]. However, because a relatively large number of elements is required for these applications, the cost of computation can be very high if the dynamics are computed via the Biot-Savart law. Alternatively, the vortex-in-cell technique, described in Section 4, may be used to compute the vortex interactions thereby significantly reducing the price of the simulation. In Section 5 we use the vortex-in-cell method to study the dynamics of perturbed Stuart vortices - a model of the mixing layer with two-dimensional structure.

2. DYNAMICAL EQUATIONS FOR VORTEX FILAMENTS

For a constant density flow, the dynamics of the vorticity field $\boldsymbol{\omega}$ is given by

$$\frac{D\boldsymbol{\omega}}{Dt} \equiv \frac{\partial \boldsymbol{\omega}}{\partial t} + \mathbf{u}\cdot\nabla\boldsymbol{\omega} = \boldsymbol{\omega}\cdot\nabla\mathbf{u} + \nu\nabla^2\boldsymbol{\omega} , \tag{1}$$

where $\mathbf{u}$ is the velocity and ν is the kinematic viscosity. From the relations $\nabla\cdot\mathbf{u} = 0$ and $\nabla\times\mathbf{u} = \boldsymbol{\omega}$ we find that

$$\nabla^2\mathbf{u} = -\nabla\times\boldsymbol{\omega} , \tag{2}$$

so that $\mathbf{u}$ may be expressed as

$$\mathbf{u}(\mathbf{r},t) = -\frac{1}{4\pi}\int \frac{(\mathbf{r}-\mathbf{r}')\times\boldsymbol{\omega}(\mathbf{r}',t)}{|\mathbf{r}-\mathbf{r}'|^3} d\mathbf{r}' + \nabla\phi , \tag{3}$$

where $\mathbf{r}$ is the space vector (x,y,z) and ϕ is the potential associated with the homogeneous solution of (2) required to satisfy boundary conditions.

For numerical purposes we assume that the vorticity may be represented as a system of vortex filaments following the three-dimensional space curves $\mathbf{r}_i(\xi,t)$, $(i = 1, 2, 3, \ldots)$ where ξ is a parameter along a given curve. The velocity field is then given by

$$\mathbf{u}(\mathbf{r},t) = -\sum_i \frac{\Gamma_i}{4\pi} \int \frac{(\mathbf{r}-\mathbf{r}_i(\xi',t)) \times (\partial \mathbf{r}_i/\partial \xi')\, g(|\mathbf{r}-\mathbf{r}_i|/\sigma_i)}{|\mathbf{r}-\mathbf{r}'|^3} \, d\xi' , \tag{4}$$

where g is a smoothing function that depends on the assumed structure of the vortex core as discussed in [8]. For the study described in the next section we used the function

$$g(c) = \frac{c^3}{(c^2+\alpha)^{3/2}} \tag{5}$$

in (4) with $\alpha = 0.413$, corresponding to Gaussian cores [7], and computed the velocities of the node points at ξ_k, (k = 1, 2, 3, ...) using

$$\frac{\partial \mathbf{r}(\xi_k,t)}{\partial t} = \mathbf{u}(\mathbf{r}(\xi_k,t)) \, . \tag{6}$$

Viscous effects are neglected except for the creation of vorticity at a no-slip boundary.

A simple way to approximate the geometry of each space curve is to use a sequence of linear segments between successive nodes. With this approximation we can obtain an exact analytical expression for the integral in (4) with g given by (5). In an improved method that we recently developed, the trapezoid rule is used to integrate along each space curve with parametric cubic splines to estimate the required derivatives $\partial \mathbf{r}/\partial \xi$ at each node. The new method requires only half the number of arithmetic operations per node point and, generally, only half the number of node points for equivalent accuracy. As an illustration, the convergence of the self-induced velocity of a vortex ring are shown in Figure 1 for the linear-segment scheme and the spline-based method as a function of the number of points. As a consequence of the savings in operation count and number of node points (for the same accuracy), the spline-based scheme is approximately a factor of eight faster.

3. SIMULATION OF THE PERTURBED ROUND JET

In a typical unperturbed, turbulent round jet, the shear layer exiting the jet nozzle rolls up into distinct vortex ring structures that eventually merge and appear to loose their coherence. In the experimental work of Lee & Reynolds [6] it was observed that small perturbations can significantly alter the development of round turbulent jets. They introduced both axial and orbital excitations. By pulsing the jet axially, they control the frequency at which the vortex ring structures are formed. The orbital excitation is produced by moving the nozzle tip in a circular orbit about the nominal centerline of the jet. If the orbital period is a small integer ($= n_r$) multiple of the period of the vortex ring formation, the jet splits into n_r distinct trains of vortex rings equally spaced around the azimuth. For $n_r = 2$, the angle between the branches, referred to as the bifurcation angle, was found to vary from 40° to 80°, depending on the Strouhal number ($St = fD/\langle U \rangle$).

In this section we investigate the dynamics of this process for $n_r = 2$, the bifurcating jet, using a three-dimensional vortex simulation with the thin-filament approximation. The important vorticity in the flow is assumed to be in the form of a semi-infinite cylindrical

sheet of azimuthal vorticity, representing the source flow, and a collection of vortex filaments as illustrated in Figure 2. The velocity field induced by the vortex sheet was defined analytically and an efficient scheme was developed for its numerical evaluation. New vortex rings are created periodically at the jet exit with a circulation consistent with the flux of circulation given by $d\Gamma/dt = 0.5U_c^2$ where U_c is the jet centerline velocity. The effect of orbital excitation is approximated in the simulation by rotating the cylindrical vortex sheet in a circular orbit about the nominal centerline of the flow.

Typical experimental and computational results are shown in Figures 3 and 4 for a case of large bifurcation angle. In the experiment, dye was injected circumferentially at the jet exit, to mark the vortex structures in the jet fluid. The computational results have shown that the axial spacing between rings, which depends inversely on St, is a crucial parameter. For the spacing that yields maximum spreading, the successive rings strongly interact at a certain downstream location, launching one another along widely separated paths (Figure 4b). If the spacing is too large, the interaction is too weak to produce wide angles (Figure 4a). If the spacing is too small, successive rings collide and merge (Figure 4c). As a consequence, one obtains a bifurcation angle that increases with St, but with low and high frequency cutoffs as shown in Figure 5a. The experimental results [6] presented in Figure 5b show a similar relationship between bifurcation angle and Strouhal number. However the maximum angles achieved in the experiment are twice those of the simulation, and the excitation amplitude is an order of magnitude less. We are currently exploring a number of possible reasons for these discrepancies. Errors due to the thin-filament approximation may be significant and the details of the flow near the nozzle may need more accurate representation. Nevertheless the vortex simulations predict the correct trends and we believe that they demonstrate that vortex interaction is the key mechanism governing the structure of the flow.

4. VORTEX-IN-CELL METHOD

As the number of vortex node points increases beyond a few thousand, the vortex method described in Section 2, a direct-interaction scheme using the Biot-Savart law, becomes prohibitively expensive, even on presently available supercomputers. In this section we discuss an alternative scheme to compute node velocities at a much lower cost. The idea is to retain the Lagrangian treatment of the vorticity field but to solve the Poisson equation for the velocity field on a fixed Eulerian mesh. By use of fast Poisson solvers on a mesh of M grid points, the operation count for this step can approach $O(M \log M)$. Additional required steps are (1) the generation of mesh values of vorticity from the Lagrangian representation and (2) interpolating velocities from the mesh back onto the Lagrangian points. Therefore the computing time per time step for the vortex-in-cell method is $O(N) + O(M \log M)$, a substantial reduction over the $O(N^2)$ time required for the direct-interaction scheme. However the vortex-in-cell scheme requires a more complex algorithm and the introduction of another layer of numerical approximation. In addition, some boundary conditions, such as the infinite domain, are more difficult to implement, while the periodic boundary condition, for example, is simpler.

In the three-dimensional vortex-in-cell method of Couët et al [3], developed for flow fields that are periodic in all three directions, the vorticity field is represented as a collection of filaments with Gaussian cross section,

$$\omega(\mathbf{r},t) = \sum_i \Gamma_i \oint \exp\left[\frac{-|\mathbf{r}-\mathbf{r}_i(\xi',t)|^2}{\sigma^2}\right] \frac{\partial \mathbf{r}_i}{\partial \xi'} d\xi' \,. \tag{7}$$

A specially developed quadratic-spline interpolation scheme is used to minimize the errors in deposition of vorticity onto the mesh and in interpolation of velocities onto the Lagrangian points. The method was used in the computation of model problems and the results were compared with solutions known to be accurate [3]. Excellent results were achieved. In the application below we use the extension of the method to the infinite domain [4], suitable for slabs of vorticity, having finite thickness in one direction.

3. DYNAMICS OF AN INHOMOGENEOUS MIXING LAYER

We apply the vortex-in-cell method, described in the previous section, to the study of the dynamics of perturbed Stuart vortices [12]. The vorticity field for the unperturbed, two-dimensional flow is periodic in the stream (x) direction with period L and is given by

$$\omega_z(x,y) = \frac{-2\pi\,(1-\rho^2)/L}{[\cosh(2\pi y/L) - \rho\cos(2\pi x/L)]^2} \,, \tag{8}$$

where $\rho \in [0,1]$ is a parameter. If $\rho = 0$, a parallel tanh shear profile is obtained and if $\rho \to 1$ one obtains a row of point vortices. At $y = \pm\infty$ the streawwise velocity is ± 1. Thus the circulation of each vortex is 2L. In the following, we study the case $\rho = 0.25$ and set $L = 16$.

To simulate the dynamics of this vorticity continuum we use an array of 16×25 vortex filaments for each Stuart vortex. Thus the spacing between filaments is $\Delta x = \Delta y = 1.0$. In the span (z) direction, 32 node points are used to define the space curve of each filament. To allow for the study of subharmonic disturbances, the computational domain includes two Stuart vortices or 800 filaments and a total of 25600 node points in a 32×3 Eulerian mesh.

Each vortex filament represents a vorticity field given by Eq.(7) with an effective core parameter σ. Therefore the circulation of each filament may be determined to minimize square error in representing the exact vorticity field given by (8). Figure 6 shows the quality of the representation that is obtained. Contours of vorticity field given by (8) are plotted together with the field obtained numerically; they are virtually indistinguishable. The rms error normalized to $<\omega_z^2>^{1/2}$ is only 0.12%. The exact unperturbed state is of course steady but the approximate vortex filament representation produces a time-dependent flow. Figure 7 shows the evolution of the unperturbed state after 380 time steps. Nearly neutral oscillations are observed with normalized rms error equal to 29%. However, the time-averaged flow remains close to the exact steady state (Figure 8) with normalized rms error equal to 5.6%.

Next we consider small three-dimensional perturbations to the Stuart vortices. The linear stability calculations of Pierrehumbert & Widnall [10] are available for comparison. In our calculations the vortices are centered at $x = 0$ and $x = 16\ (= -16)$. Thus by displacing the vortex node points in the x - y plane at $t = 0$ by the amount

$$\delta x = \delta y = \epsilon \cos\left(\frac{\alpha \pi x}{16}\right) \cos\left(\frac{\beta \pi y}{16}\right) . \tag{9}$$

where ϵ is a small parameter, we obtain the pairing instability for $\alpha = 1$ and the translative instability for $\alpha = 0$, as studied in [10] for spanwise wavenumbers $\beta = 0, 1, 2, \cdots$.

We expect that after an initial period of adjustment the most amplified mode, if one exists, will dominate the perturbation for intermediate times and yield an exponential growth rate. At later times nonlinear effects should play a role in the dynamics. These features are displayed in Figure 9 where we show the energy in mode $\beta = 1$ for the initial disturbance $\alpha = 1, \beta = 1$. In Figure 10 we plot the exponential growth rates for this case and several others along with the results of Pierrehumbert & Widnall [10]. The agreement for small β is good to within a few per cent. Nakamura et al [9] observed errors of a similar magnitude in their study of the growth rates of $\beta = 0$ perturbations to parallel shear flows using a two-dimensional vortex method with similar resolution. In the translative instability (Figure 10a), the agreement for larger β is not good quantitatively but shows the same leveling off to a broad plateau. For the $\alpha = 1$ mode (Figure 10b) Pierrehumbert & Widnall observed a high β cutoff to the pairing instability, whereas the present results suggest a broader domain of instability. One obvious possibility for these discrepancies is insufficient resolution in the present results which causes a twofold problem. First, the unperturbed state does not consist of the exact, steady Stuart vortices, but is time-dependent (recall Figure 7) and, second, the resolution of the perturbation state must rely on the relatively coarse grid that is used. Another possibility is that, in our simulation, a branch to another family of unstable modes has taken place as β is increased - a family that has more complex structure in the vortex core. Finite area vortices (ellipses), when subjected to an external strain field, are subject to an infinite hierarchy of instabilities as $\beta \to \infty$ [11,13]. If the strain is low, the unstable domains in β are separated by neutrally stable domains. For higher strain, the unstable domains completely overlap. Further work is needed to establish whether such a hierarchy exists for the Stuart vortices. We suspect that it does and that we have encountered such a higher mode instability, but at the possibly incorrect wavenumber. In Figure 11 we show contours of $\omega_z - \omega_{z_0}$, where ω_{z_0} is the computed vorticity field for the unperturbed initial condition ($\epsilon = 0$). Figure 11a illustrates the mode shape for the pairing instability $\alpha = 1, \beta = 0$ after 380 time steps. The mode profile agrees qualitatively with that given in [10] for the same spanwise wavenumber. Figure 11b illustrates the mode shape for the translative instability $\alpha = 0, \beta = 1$; the structure here appears more complex but the results are not conclusive.

Of course the primary advantage of the present method is that fully nonlinear studies of three-dimensional inviscid flows are possible. Figure 12 shows the energies of the various

spanwise modes in the nonlinear regime for the cases $\alpha = 0$, $\beta = 2$ and for $\alpha = 1$, $\beta = 1$. As seen from the visualization of the vortex filaments in Figure 13, the vortex cores are starting to overlap when $t = 300$ and the vortex shape deviates noticeably from a sinusoid when $t = 400$. Studies of more complex physical problems are planned, including vortex ring interactions with Stuart vortices.

6. CONCLUSIONS

Three-dimensional vortex methods, employing Lagrangian elements of vorticity, are well suited to the study of many complex flows at high Reynolds numbers. When the flow consists mainly of isolated tubes of vorticity, a single computational filament may be assigned to each physical vortex and the dynamics computed via the Biot-Savart law at a reasonable cost. Simulations of the perturbed round jet were performed with this scheme and have shown that three-dimensional vortex interactions between successive vortex rings are responsible for the observed bifurcation of the jet fluid.

If the physical vortex tubes undergo collision, merging, or any other process in which the structure of the vortex core is important to the dynamics, a large number of computational elements must be used to represent each vortex. In many cases the vortex-in-cell method may be used to reduce substantially the cost of computation. In this paper, the vortex-in-cell method was used to study the linear and nonlinear three-dimensional vortex interactions of perturbed Stuart vortices, a flow field that is representative of an inhomogeneous mixing layer.

Acknowledgment

The authors wish to thank M. J. Lee and W. C. Reynolds for their many contributions to the study of the perturbed jet and the Air Force Office of Scientific Research for their support of the round jet simulations under Contract AF K-0005.

References

1. ANDERSON, C. and GREENGARD, C., "On Vortex Methods", SIAM Journal on Numerical Analysis, 22, 1985.

2. BEALE, J.T. and MAJDA, A., "Vortex Methods I: Convergence in Three Dimensions", Mathematics of Computation, 39, 1982, pp. 29-52.

3. COUET, B., BUNEMAN, O., and LEONARD, A., "Simulation of three- dimensional incompressible flows with a vortex-in-cell method", Journal of Computational Physics, 39, 1981, pp. 305-328.

4. COUET, B. and LEONARD, A., "Exact Extension to the Infinite Domain for the Vortex-in-cell Method", SIAM Journal on Scientific and Statistical Computing, 2, 1981, pp. 311-320.

5. GREENGARD, C., "Convergence of the Vortex Filament Method", submitted for publication, 1985.

6. LEE, M.J. and REYNOLDS, W.C.,"Structure of the Bifurcating Jet", Bulletin of the American Physical Society, 28, 1983, p. 1362.

7. LEONARD, A.,"Vortex Methods for Flow Simulation", Journal of Computational Physics, 37, 1980, pp. 289-335.

8. LEONARD, A.,"Computing Three-Dimensional Incompressible Flows with Vortex Elements", Annual Review of Fluid Mechanics, 17, 1985, pp. 523-559.

9. NAKAMURA, Y., LEONARD, A., and SPALART, P.,"Vortex Simulation of an Inviscid Shear Layer", AIAA-82-0948, 1982.

10. PIERREHUMBERT, R.T. and WIDNALL, S.E.,"The Two- and Three-dimensional Instabilities of a Spatially Periodic Shear Layer", Journal of Fluid Mechanics, 114, 1982, pp. 59-82.

11. ROBINSON, A.C. and SAFFMAN, P.G.,"Three Dimensional Stability of an Elliptical Vortex in a Straining Field", Journal of Fluid Mechanics, 142, 1984, pp. 451-466.

12. STUART, J.T.,"On Finite Amplitude Oscillations in Laminar Mixing Layers", Journal of Fluid Mechanics, 29, 1967, pp. 417-440.

13. TSAI, C-Y. and WIDNALL, S.E.,"The Stability of Short Waves on a Straight Vortex Filament in a Weak Externally Imposed Strain Field", Journal of Fluid Mechanics, 73, 1976, pp. 721-733.

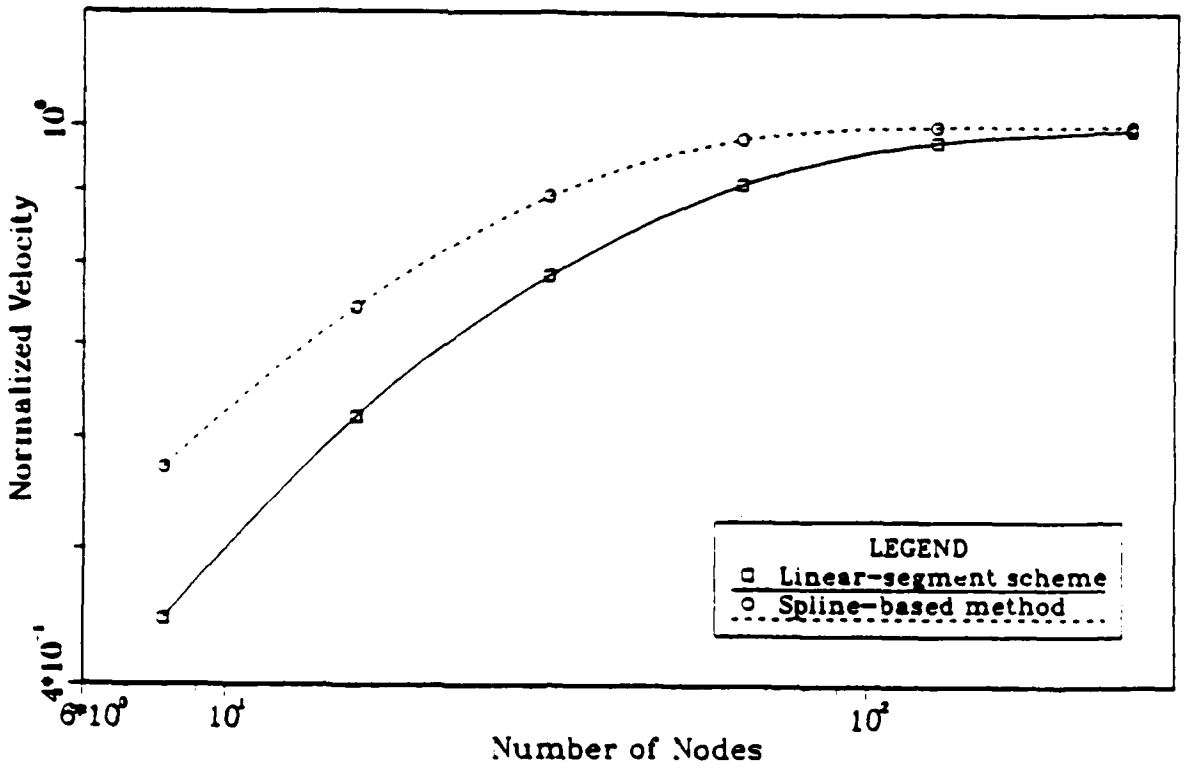

Figure 1 Convergence of the speed of a vortex ring as the number of nodes is increased. $\sigma/R = 0.1$.

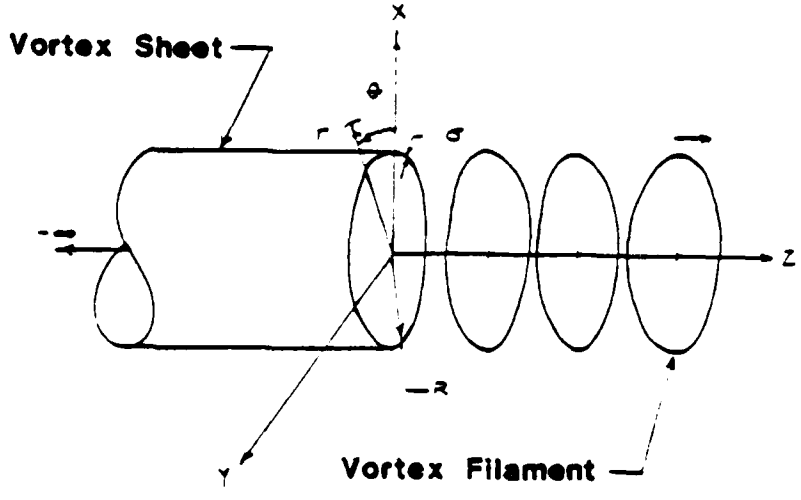

Figure 2 Schematic of the computational vortex elements used in the simulation of the perturbed round jet.

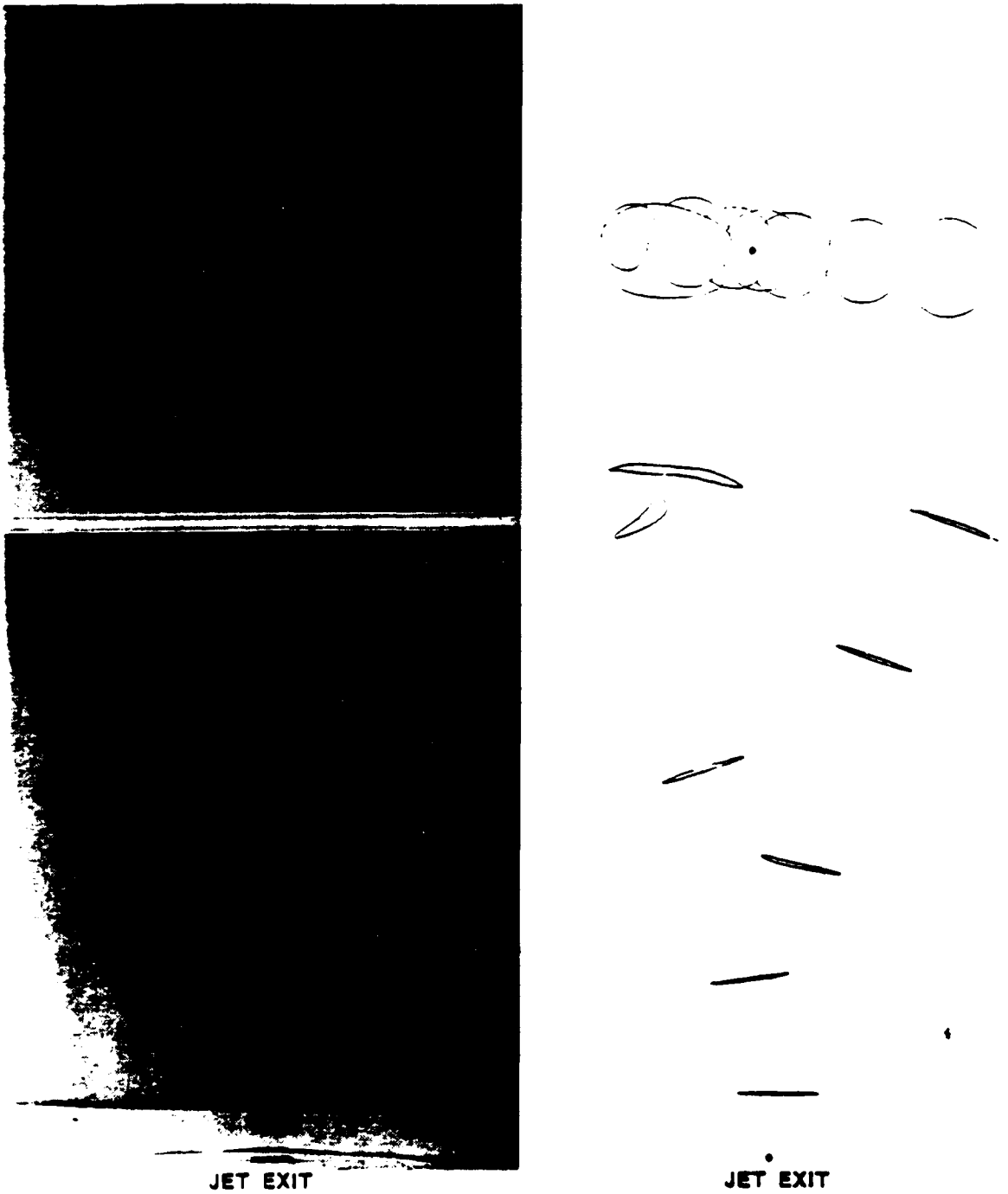

Figure 1 Bifurcation round jet, excited axially and orbitally. (Left) Experiment of Lee & Reynolds; (right) present vortex simulation. (top) front views; (bottom) side views

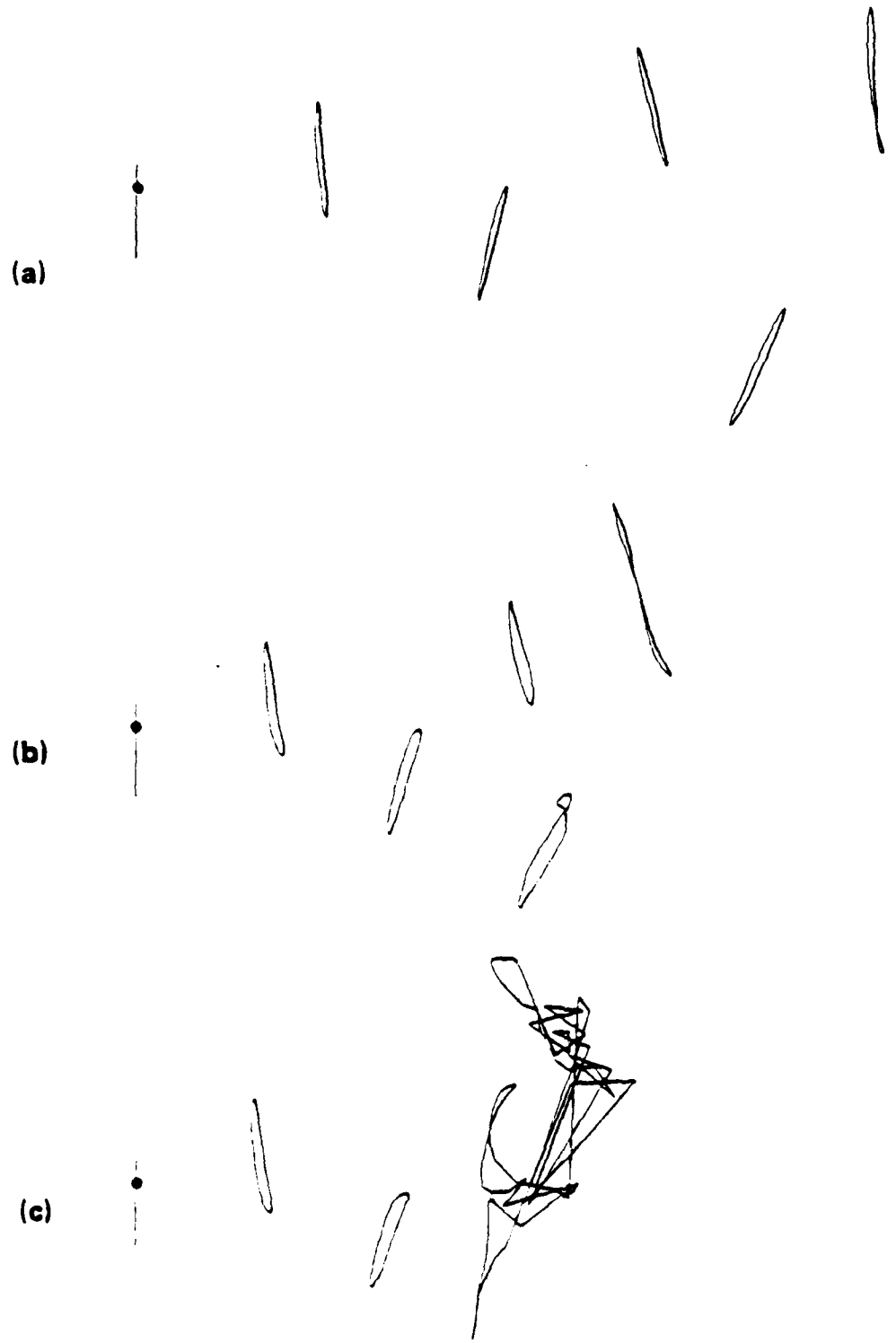

Figure 4 Dependence of the structure of the jet on Strouhal number. (a) St = 0.35, (b) St = 0.42, (c) St = 0.45.

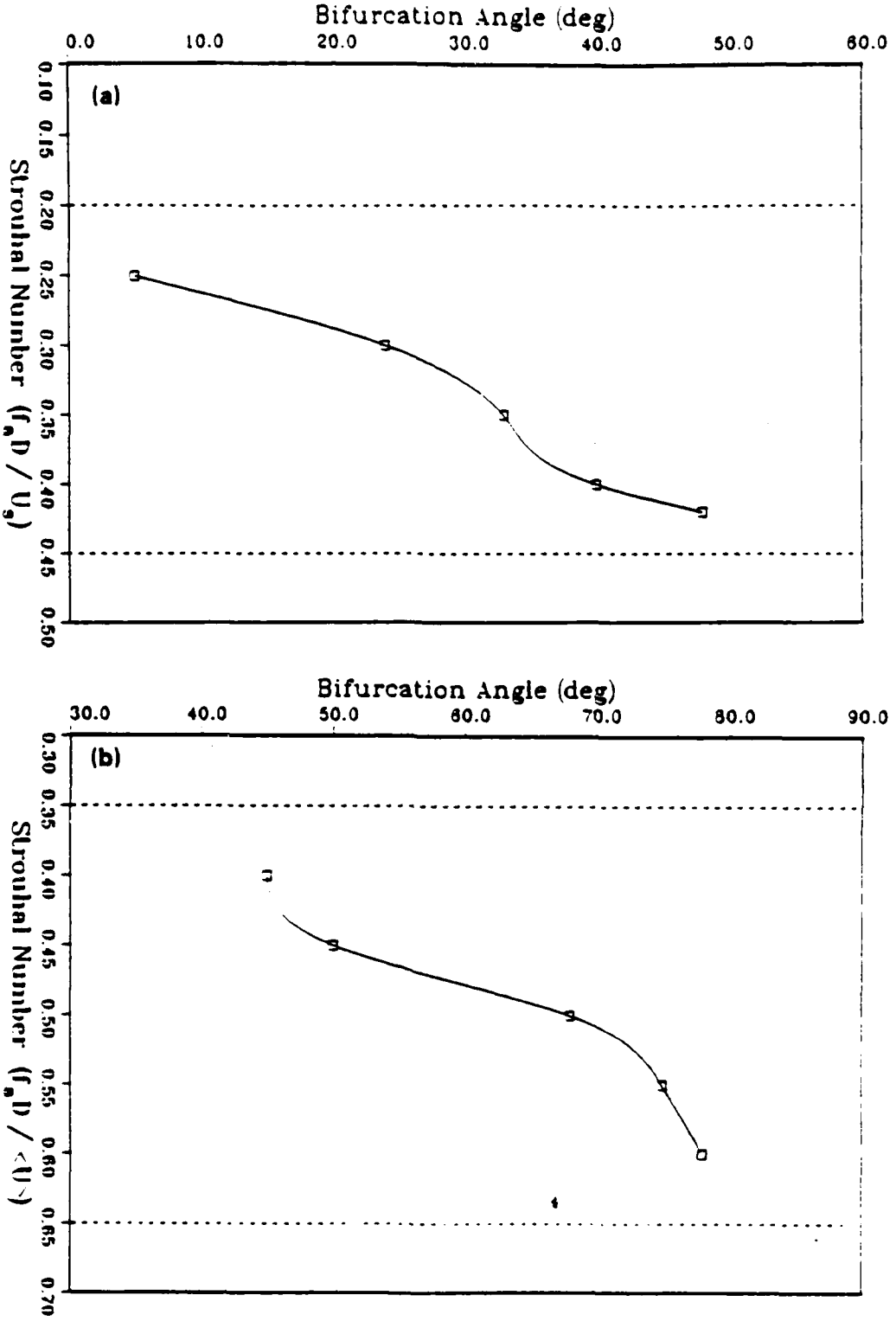

Figure 5 Bifurcation angle versus Strouhal number. Dashed lines give the boundaries of the bifurcation mode. (a) present simulations; (b) experiment [6].

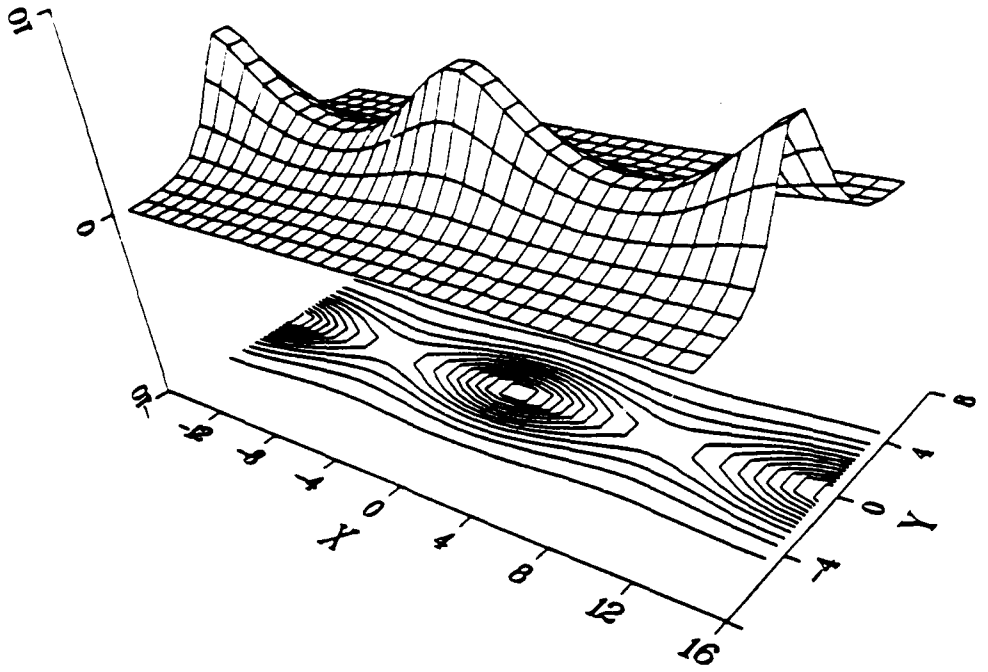

Figure 6 Contours of analytic vorticity and their 2-D projection together with computed vorticity at initial time. Increment in 2-D contour levels = 0.05.

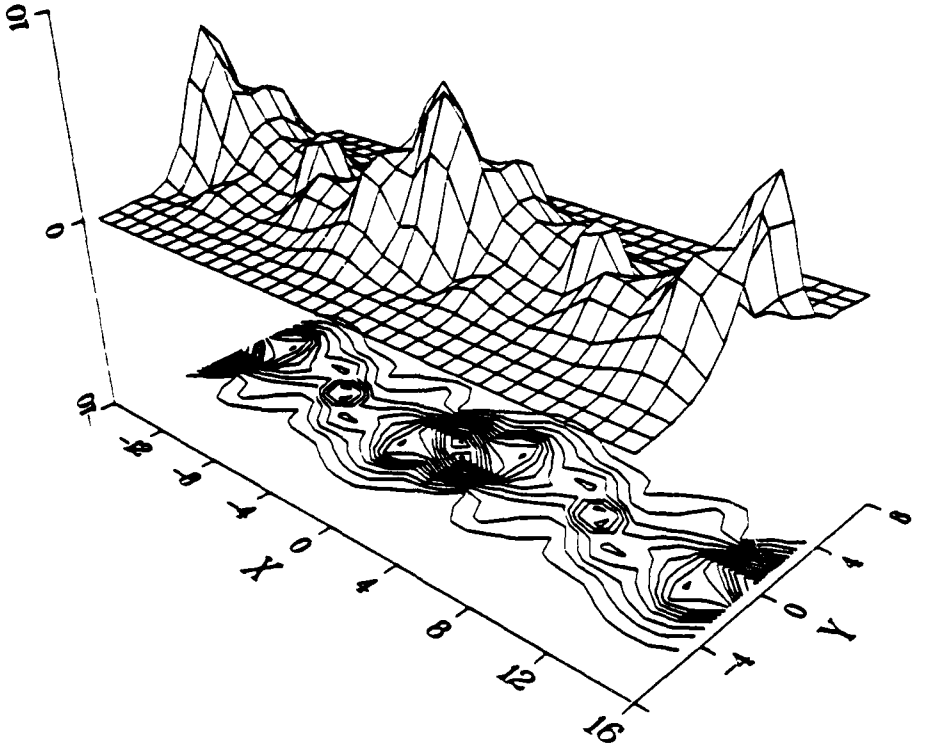

Figure 7 Contours of computed vorticity and their 2-D projection after 380 time steps. Increment in 2-D contour levels = 0.05.

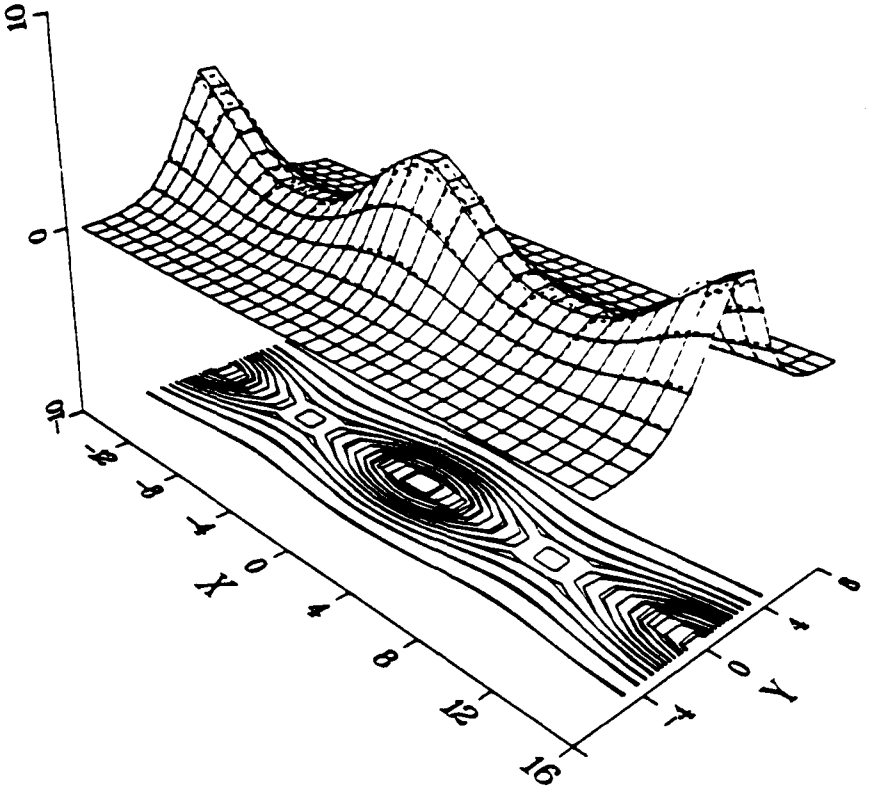

Figure 8 Contours of analytic vorticity and their 2-D projection together with the time-averaged computed vorticity (dashed) after 384 time steps. Increment in 2-D contour levels = 0.05.

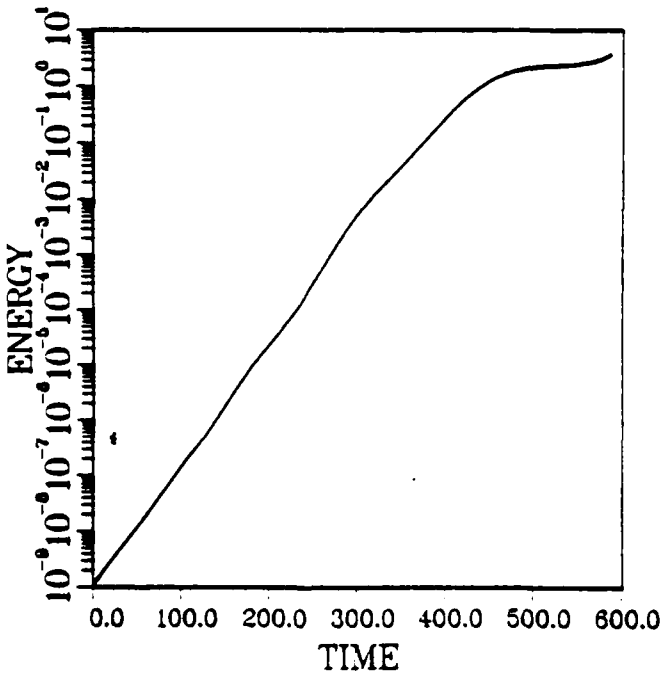

Figure 9 Time evolution of total energy in mode $\beta = 1$ for the initial disturbance $\alpha = 1.\ \beta = 1$

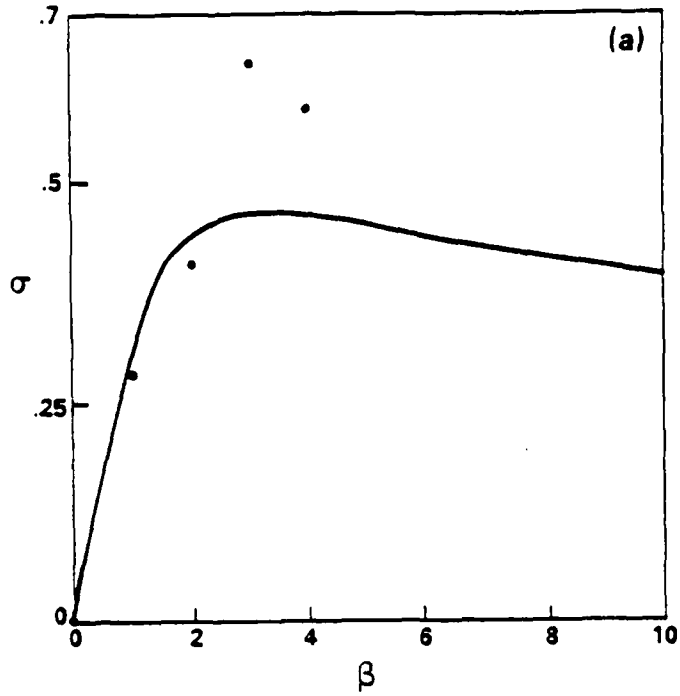

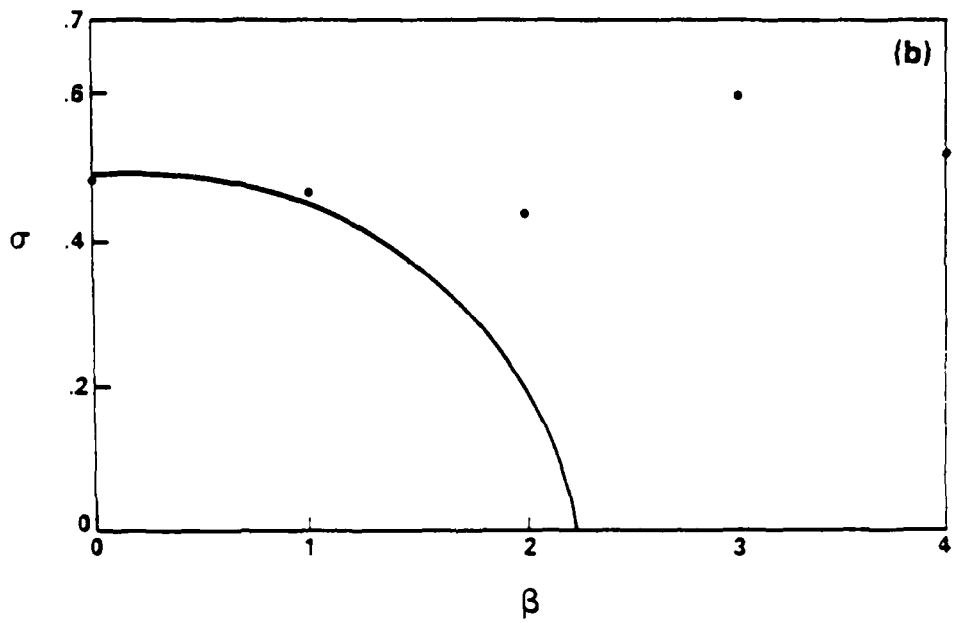

Figure 10 Growth rate versus β for (a) $\alpha = 0$ and (b) $\alpha = 1$. Solid lines from Pierrehumbert & Widnall [10] while the dots are the present simulations.

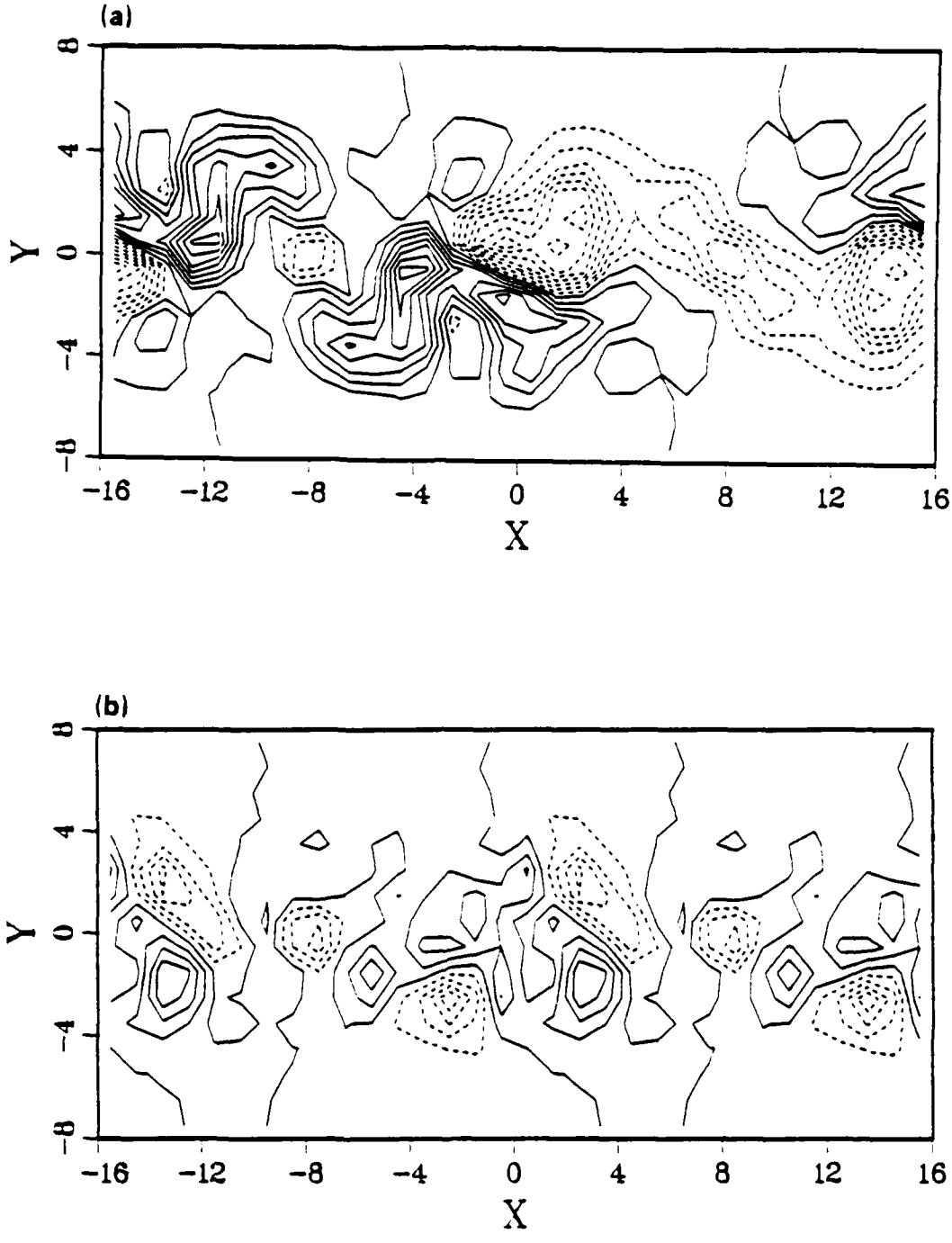

Figure 11 Contours of perturbation ω_z after 380 time steps. Dashed lines for positive contours and solid lines for negative contours. Increment in levels = 0.05. (a) $\alpha = 1$, $\beta = 0$; (b) $\alpha = 0$, $\beta = 1$.

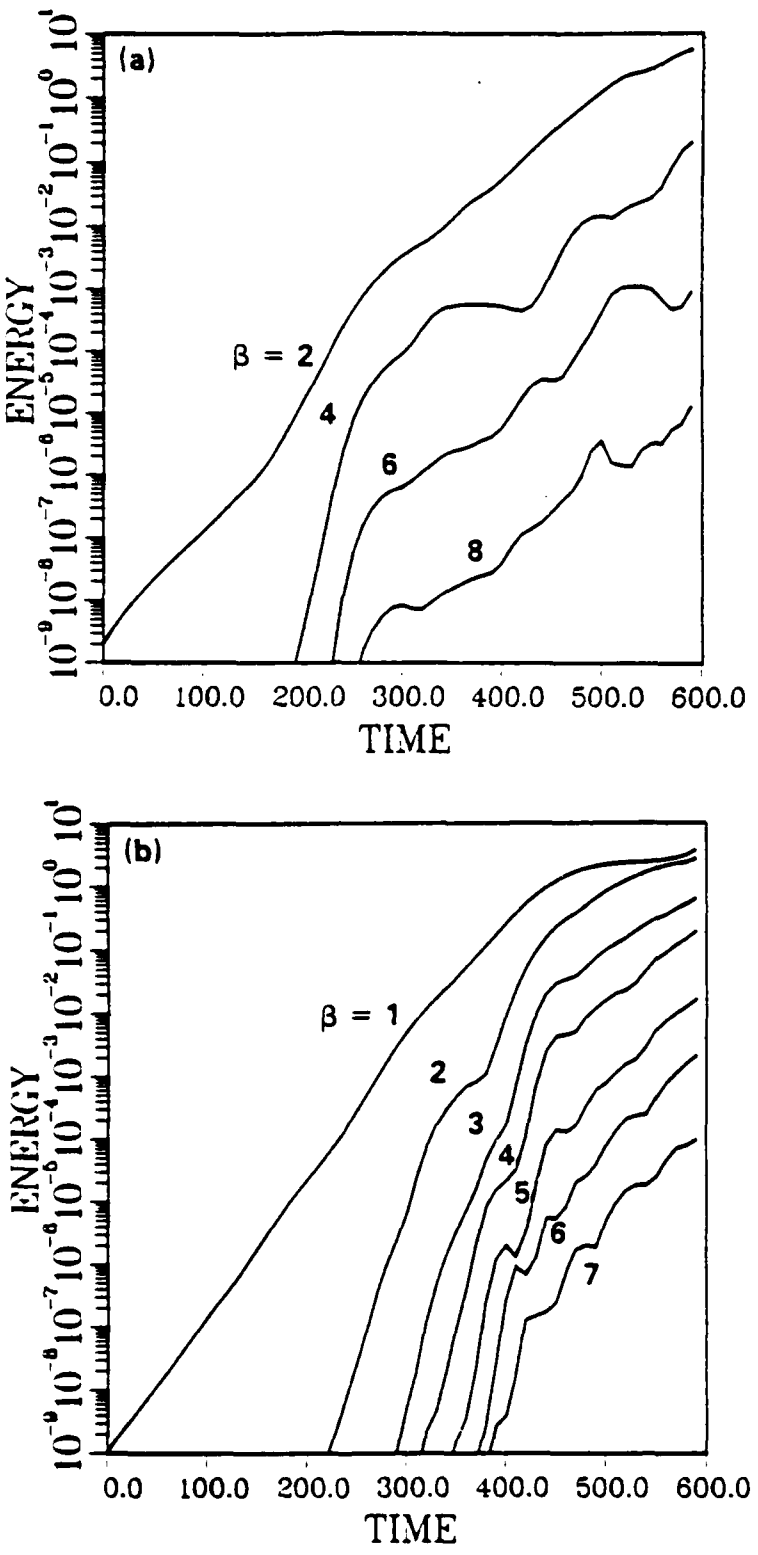

Figure 12 Time evolution of total energy for various spanwise modes for the initial disturbances (a) $\alpha = 0$, $\beta = 2$ and (b) $\alpha = 1$, $\beta = 1$.

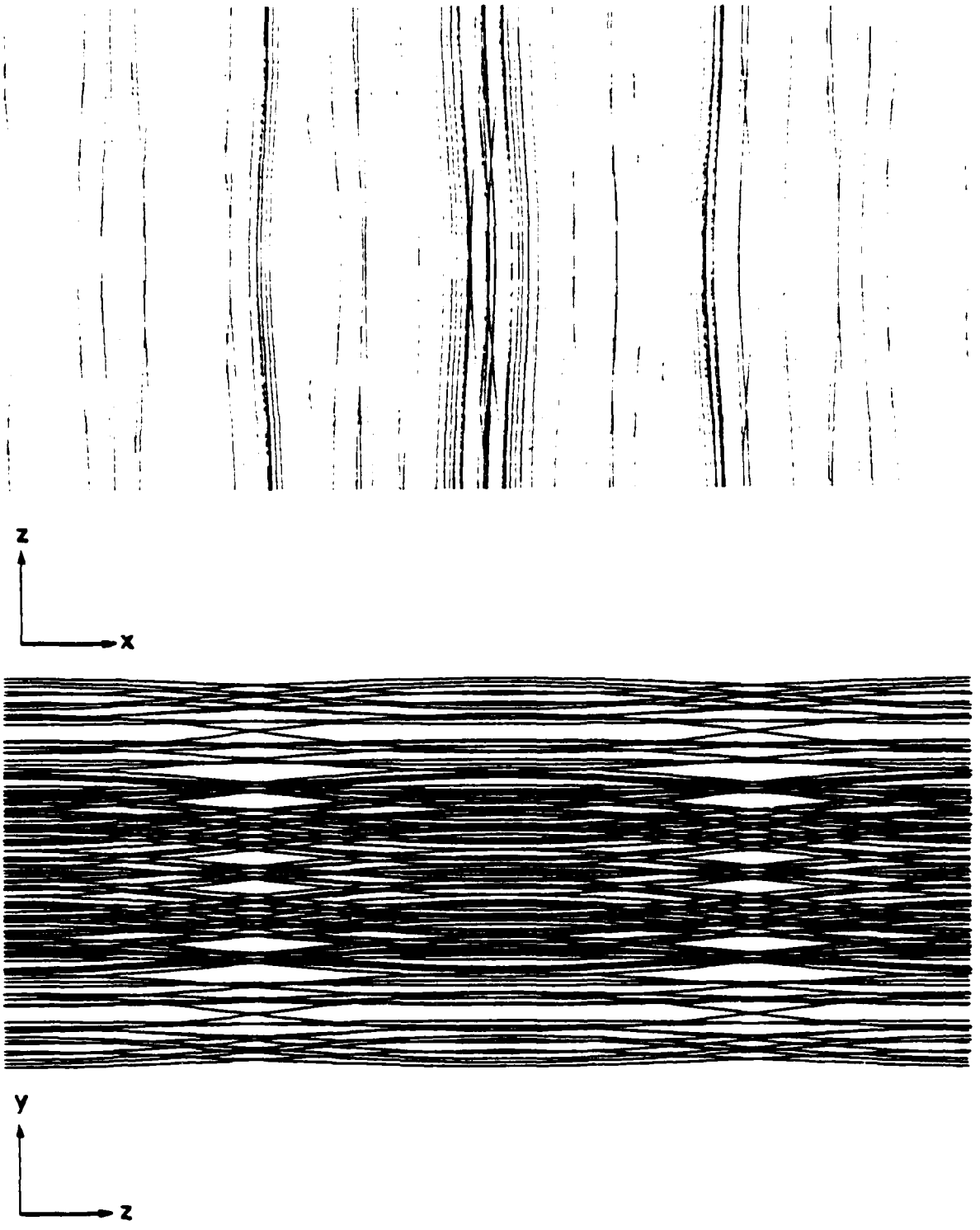

Figure 13a. After 300 time steps, five layers of filaments extending from x = -15 to 15, y = -2 to 2 and z = -15 to 15

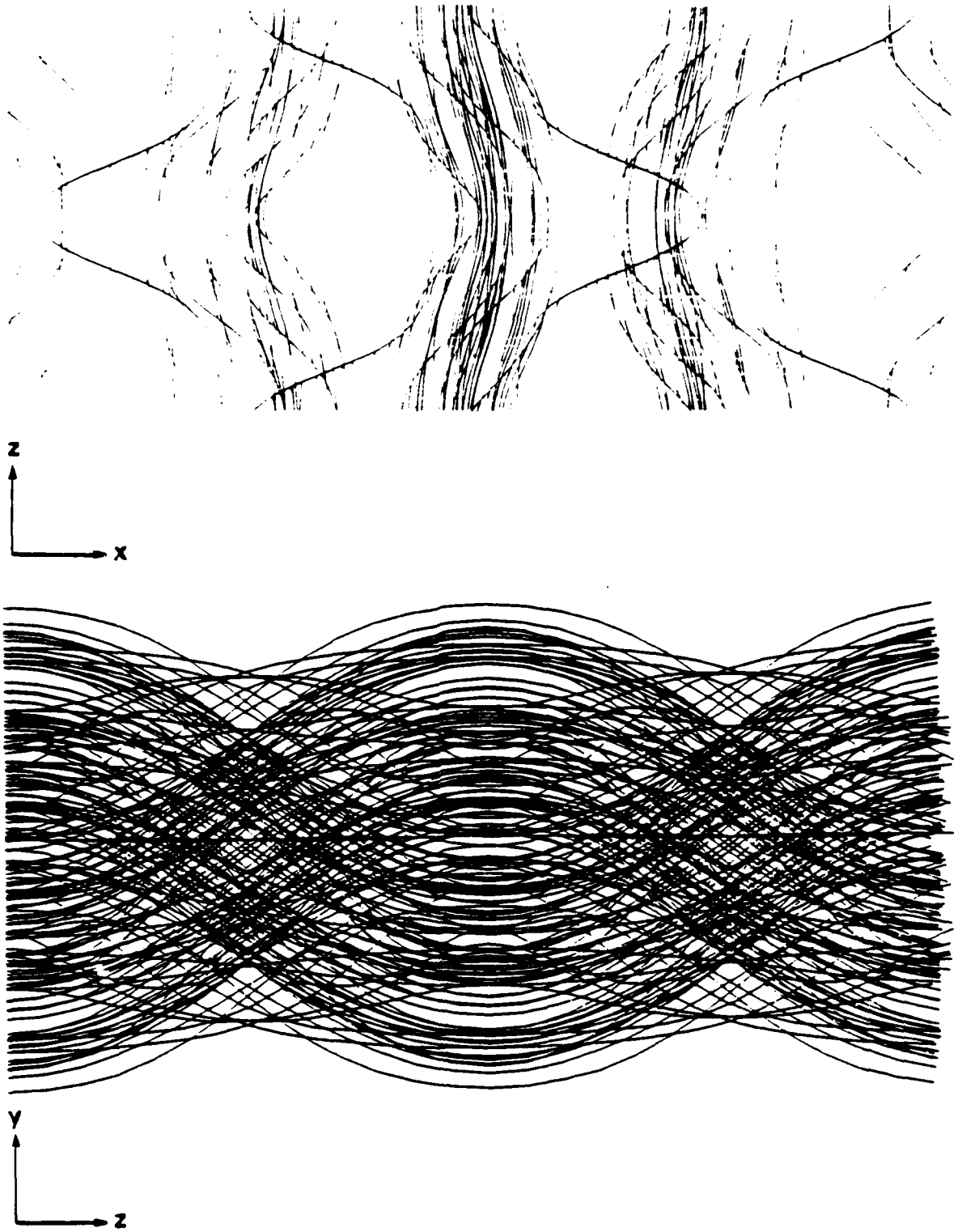

Figure 13b After 400 time steps, five layers of filaments extending from x = -15 to 16, y = -2 to 2 and z = -15 to 16

AIAA'87

AIAA-87-0164

Bifurcation of Round Air Jets by Dual-Mode Acoustic Excitation

D. E. Parekh, W. C. Reynolds,
and M. G. Mungal
Stanford University, Stanford, CA

AIAA 25th Aerospace Sciences Meeting

January 12-15, 1987/Reno, Nevada

BIFURCATION OF ROUND AIR JETS BY DUAL-MODE ACOUSTIC EXCITATION

D. E. Parekh[a], W. C. Reynolds[b], and M. G. Mungal[c]
Department of Mechanical Engineering
Stanford University, Stanford, CA 94305-3030

Abstract

The response of circular air jets to combined streamwise and transverse acoustic excitation is described. The jet evolution and structure are documented by flow visualisation. When the ratio of axial to transverse excitation frequencies is two, the jet "bifurcates" into two distinct jets. The spreading angle increases dramatically with excitation amplitude.

Nomenclature

A	excitation amplitude, p'/Z_0U
D	nozzle exit diameter
f	excitation frequency
L	sound pressure level
p'	acoustic pressure
R	f_a/f_t
Re	Reynolds number, UD/ν
St	Strouhal number, f_aD/U
U	mean exit velocity
Z	acoustic impedance
ν	kinematic viscosity
Subscripts	
a	axial
0	ambient
t	transverse

Introduction

The shear layer of a jet naturally rolls up into distinct vortex rings due to the Kelvin-Helmholtz instability. These rings combine to form larger structures which also pair or breakdown. This process of vortex formation and pairing is somewhat random in the unexcited jet. However, by proper axial excitation one can control the frequency at which the vortices form and subsequently pair. This is true for both the thin, closely-spaced rings near the exit as well as for the larger rings.[1] Furthermore, one can use this single-mode forcing to control jet growth by enhancing or suppressing vortex pairing.[2]

a Research Assistant, Mechanical Engineering Student Member, AIAA
b Professor, Mechanical Engineering Associate Fellow, AIAA
c Assistant Professor, Mechanical Engineering Member, AIAA

This vortex pairing process has also been studied in the mixing layer, where it was found that forcing at a subharmonic of the most amplified frequency results in the amalgamation of several vortices.[3] Only very low levels of forcing are required to cause this interaction. This pairing mechanism is known as a "collective interaction".

The study of excited jets has not been limited to single- frequency plane wave excitation. A study of active cancellation of pure tones in jets involved simultaneous perturbations at two frequencies.[4] The amplification of higher order modes and their contribution to broadband jet noise has also been considered.[5,6,7] Other studies of excited jets have focused on high-speed jets[8] and jets issuing from asymmetric nozzles[9].

Properly combining axial and azimuthal modes can dramatically alter the structure and momentum transport of round jets.[10] This type of dual-mode forcing can cause a jet to split into two distinct streams (bifurcating jet) or to explode into a shower of vortex rings (blooming jet). Bifurcating jets occur when the ratio (R) of the axial to transverse frequency is two. When R is a non-integer between 1.6 and 3.2, blooming jets are observed. These phenomena occur only within a small range of Strouhal numbers, and within that range the spreading angle increases with St. These dramatic changes in jet development were discovered through a previous experiment in water at a Reynolds number of 4,000.[11] A vortex-filament simulation of bifurcating jets suggested the Strouhal number effect and identified vortex interactions as a key mechanism in this flow.[12]

Potential applications of this dual-mode excitation involve air jets at higher Reynolds numbers. Thus, this work extends the study of bifurcating and blooming jets to air flows. The objective here is to control jet flows through properly organizing the vortex structures and to study the influence of excitation amplitudes.

This paper focuses specifically on bifurcating jets at Re of 10,000 and 20,000. The acoustic excitation system and flow visualization technique are described. Finally, some preliminary results on the influence of excitation amplitudes are discussed.

Experimental Apparatus and Approach

Flow System

The experimental apparatus is shown schematically in Fig. 1. Air flows through a porous bronze cylin-

der into the plenum and is directed through a honeycomb disk upstream of the nozzle. A plexiglas coupling rigidly attaches the nozzle to the plenum. The nozzle exit diameter is 2.15 cm, and the area contraction ratio is 25 to 1. The mean exit velocities are 7 and 14 m/s, which correspond to Reynolds numbers of 10,000 and 20,000, respectively. The streamwise turbulence intensity, measured with a hot-wire on the centerline of the exit plane, is 1% of the mean exit velocity. The shear layer thickness, measured with a hot-wire 0.1 diameter from the exit, is 3% of the diameter at Re of 10,000.

Flow Visualization

The plexiglas coupling shown in Fig. 1 also serves as the passage for smoke injection. Cigar smoke enters through four ports into the coupling and forms a thin cylindrical sheet as it exits from the annular slot in a direction tangential to the core flow. Alternately, smoke can be channeled through only two opposite ports to provide an approximate cross-section of the jet. By injecting smoke into the boundary layer, instead of seeding the entire jet, one clearly marks the shear layer and vortex structures.

Both time-averaged and instantaneous pictures of the flow are taken. Time-averaged pictures are obtained by strobe illumination. The strobe is triggered at a submultiple of the excitation frequency and is thus able to phase-lock the evolution of the vortex structures. The images are recorded by a video camera. A 10-watt, copper-vapor, pulsed laser is focused into a thin sheet to provide instantaneous cross-sections of the jet. The laser is triggered to provide one pulse for each exposure taken with a 35mm camera and standard print film (ASA 400). Since the pulse duration is only 30 ns, this technique provides detailed images of even high speed flows.

Acoustic Excitation

The bifurcating jet experiment in water used a mechanical excitation system operating at frequencies around 10 Hz.[11] A diaphragm on the piston driving the flow produced the axial perturbation. The azimuthal mode was introduced by moving the nozzle tip in a small circular orbit about the nominal jet centerline. From the definitions of the Reynolds and Strouhal numbers, the excitation frequency can be written as $f_a = \nu ReSt/D^2$. This shows that switching from water to air, while keeping Re, St, and D constant, requires an order of magnitude increase in f_a.

Since the frequencies required in this experiment are several hundred hertz, an acoustic excitation system was developed. Loudspeakers produce both the axial and transverse excitations. A speaker mounted on the bottom of the plenum generates the streamwise excitation. Four external speakers (Morel, 15-cm woofers, 150W) surrounding the nozzle provide the cross-stream excitation. By mounting these speakers in the plane of the nozzle exit, one presents a flat surface to the entrained flow.

The input signals of the external speakers are sine waves of equal frequency and amplitude but different phase. The signal of a speaker differs from that of an adjacent one by 90°. The signal of the opposite speaker is 180° out of phase. The input of the internal speaker is a sine wave of a different frequency, and its phase relative to the set of four speakers is variable.

One pair of opposite external speakers is sufficient to generate the transverse forcing required to produce the bifurcating jet. However, the jet will split only if the phase shift between the pair of external speakers and the internal one is properly set. The peaks of the transverse excitation must coincide with the peaks of the axial forcing. With all four external speakers on, the phase shift simply determines the diametrical plane in which the jet bifurcates. The results reported here are produced with only the internal speaker and one external pair of opposite speakers properly phased. No signal is fed into the other pair.

The sound pressure levels are measured with a 2.4 cm microphone centered one diameter from the jet exit and oriented perpendicular to the plane containing the speaker pair. The purpose of this measurement is to specify the excitation amplitudes and not to obtain the acoustic response of the excited jet. In order to determine the forcing amplitude prior to amplification by jet instability mechanisms, all acoustic measurements are made with no flow. The two modes of excitation are measured separately. The transverse excitation amplitudes that are reported are those resulting from both speakers. The corresponding transverse amplitude from a single speaker is typically 15 dB higher than that of the pair due to the absence of cancellation by the other speaker.

The spreading angles are determined from the flow visualization. When instantaneous pictures are used, several realizations are compared to determine the angle. The spreading angle of the bifurcating jet is defined as the angle formed by the outer edges of the two branches of the jet.

Results and Discussion

The results discussed here are of a preliminary nature, yet they provide valuable insight into the structure and amplitude dependence of bifurcating jets. The Strouhal number, defined as $f_a D/U$, is around 0.6 in all these cases. This value of St was found in previous work to produce the largest spreading angles.[11] The non-dimensional amplitudes, A_a and A_t, are defined as the fluctuating acoustic velocity divided by the mean jet velocity. The acoustic velocity is *estimated* by dividing the measured acoustic pressure by the characteristic impedance of air. Thus, A_a and A_t are defined as p'_a/Z_0U and p'_t/Z_0U, respectively.

With both excitations off, we simply observe the natural jet whose shear layer rolls up into vortices in an irregular manner (Fig. 2). Turning the axial excitation on locks the vortex roll-up to the forcing frequency as seen in Fig. 3.

Cross-sections through the center of the jet show interesting differences in jet response to A_a. At low levels of streamwise forcing, one controls the vortex formation frequency by causing a periodic collective interaction of the thin closely- spaced rings near the jet exit. The axially-pulsed jet at $A_a = 0.03\%$ ($L_a = 99$ dB) is an example of this (Fig. 4). At higher levels, $A_a = 0.12\%$ ($L_a = 105$ dB), the thin vortex rings are no longer visible, and instead, one sees the initial formation of rings whose spacing is on the order of the jet diameter (Fig. 5). The stronger excitation causes a tight roll-up of the shear layer. The structure of the vortex core shows many interfaces between the jet fluid and the entrained fluid. Several diameters from the exit, vortex cores exhibit deformation and elongation due to the pairing process. The same amplitude dependence is seen in jets having the same Reynolds number, in which case the thickness of the shear layer is not an issue.

The bifurcating jet has a strikingly different structure. Figure 6 displays a cross-section of a bifurcating jet in the plane of bifurcation at $Re = 10,000$ and $St = 0.55$. The jet appears similar to an axially-excited jet near the exit except for the slight displacement and tilt of the vortices. Farther downstream, however, the flow abruptly splits into two distinct jets with an included angle of 70°. Initially adjacent vortex rings propagate along different branches of the jet. This results in the jet fluid being stretched back and forth between the two branches of the jet. Similar behavior is seen at $Re = 20,000$ (Fig. 7). Since the Reynolds number is higher and amplitudes are lower, the vortex cores are not as distinctly organized and the jet becomes fully turbulent sooner.

Changes in spreading angle due to different transverse amplitudes are seen in Fig. 8. At low amplitudes the vortices appear to be displaced laterally rather than distributed on two separate branches. The angles corresponding to different levels of axial and transverse forcing are compared in Fig. 9. Increasing A_t while keeping A_a fixed causes the spreading angle to increase from 24° up to 52°. Increasing A_a results in angles as high as 70°.

Though more data would be required to form an empirical relation between angle and amplitude, these results provide the first insights into the nature of that dependence. The spreading angle clearly increases with both amplitudes. One would intuitively expect the angle to increase with A_t since that perturbation is aligned with the direction of bifurcation. The fact that the angle dramatically increases with A_a would be harder to anticipate. It appears that higher values of A_a concentrate the vorticity in the shear layer more strongly. Thus, the vortices are less diffuse and probably have a higher circulation. This, in turn, amplifies the vortex interactions, resulting in wider spreading angles. One would expect to reach a saturation level beyond which the angle no longer increases with either amplitude. However, that level did not appear to be reached in these experiments.

These results confirm and expand the previous understanding of the governing mechanisms in this flow. The bifurcation phenomenon has been regarded as the result of vortex interactions.[11,12] Eccentric rings mutually induce each other to tilt away from the centerline. This process amplifies until the jet becomes two separate trains of collinear rings. The present results are in agreement with that model. Additionally, this experiment demonstrates that the vortex interactions can be intensified by increasing either excitation amplitude.

Conclusions

An acoustic excitation system capable of generating both streamwise and cross-stream perturbations was developed for round air jets. The effect of this dual-mode forcing at different Reynolds numbers and excitation amplitudes is visually documented. These results demonstrate that dual-mode excitation can cause a jet to split into two distinct jets with a spreading angle as high as 70°. The Reynolds number range for bifurcation has been extended to as high as 20,000 with excitation frequencies up to 386 Hs.

This experiment agrees with previous understanding of the bifurcating jet structure and past models of the vortex interactions. Additionally, this work shows that the spreading angle of the bifurcating jet increases with both axial and transverse amplitudes.

Acknowledgments

This work was sponsored by the Air Force Office of Scientific Research under Contract AF-F49620-84-K-0005.

References

1. Zaman, K. B. M. Q., and A. K. M. F. Hussain, "Vortex Pairing in a Circular Jet under Controlled Excitation," *J. Fluid Mech.*, pp. 449-491 (1980).

2. Bouchard, E. E., and W. C. Reynolds, "The Effects of Forcing on the Mixing-Layer Region of a Round Jet," Unsteady Turbulent Shear Flows, IUTAM Sym., pp.370-379 (1981).

3. Ho, C. M., and L. S. Huang, "Subharmonics and Vortex Merging in Mixing Layers," *J. Fluid Mech.*, pp. 443-473 (1982).

4. Arbey, H., and J. E. Ffowcs Williams, "Active Cancellation of Pure Tones in an Excited Jet," *J. Fluid Mech.*, pp. 445-454, (1984).

5. Bechert, D. W., and E. Pfizenmaier, "Amplification of Jet Noise by a Higher-Mode Acoustical Excitation," *AIAA J.*, vol. 15, no.9, pp.1268-1271 (1977).

6. Betsig, R. E., "Experiments on the Linear and Non-Linear Evolution of the Double Helical Instability in Jets," AIAA paper 81-0415 (1981).

7. Strange, P. J. R., and D. G. Crighton, "Spinning Modes on Axisymmetric Jets. Part 1.",*J. Fluid Mech.*, pp. 231-245 (1983).

8. Lepicovsky, J., K. K. Ahuja, W. H. Brown, and P. J. Morris, "Acoustic Control of Free Jet Mixing", AIAA paper 85-0569 (1985).

9. Kibens, V., and R. W. Wlesien, "Active Control of Jets from Indeterminate-Origin Nozzles," AIAA paper 85-0542 (1985).

10. Lee, Mario, and W. C. Reynolds, "Bifurcating and Blooming Jets," Fifth Symposium on Turbulent Shear Flows, pp. 1.7-1.12 (1985).

11. Lee, Mario, and W. C. Reynolds, "Bifurcating and Blooming Jets," Report TF-22, Thermosciences Divisioin, Dept. of Mech. Engr., Stanford University, (1985).

12. Parekh, D. E., A. Leonard, and W. C. Reynolds, "A Vortex- Filament Simulation of a Bifurcating Jet," Bulletin of the Amer. Phys. Soc., vol. 28, no. 9, p. 1353 (1983).

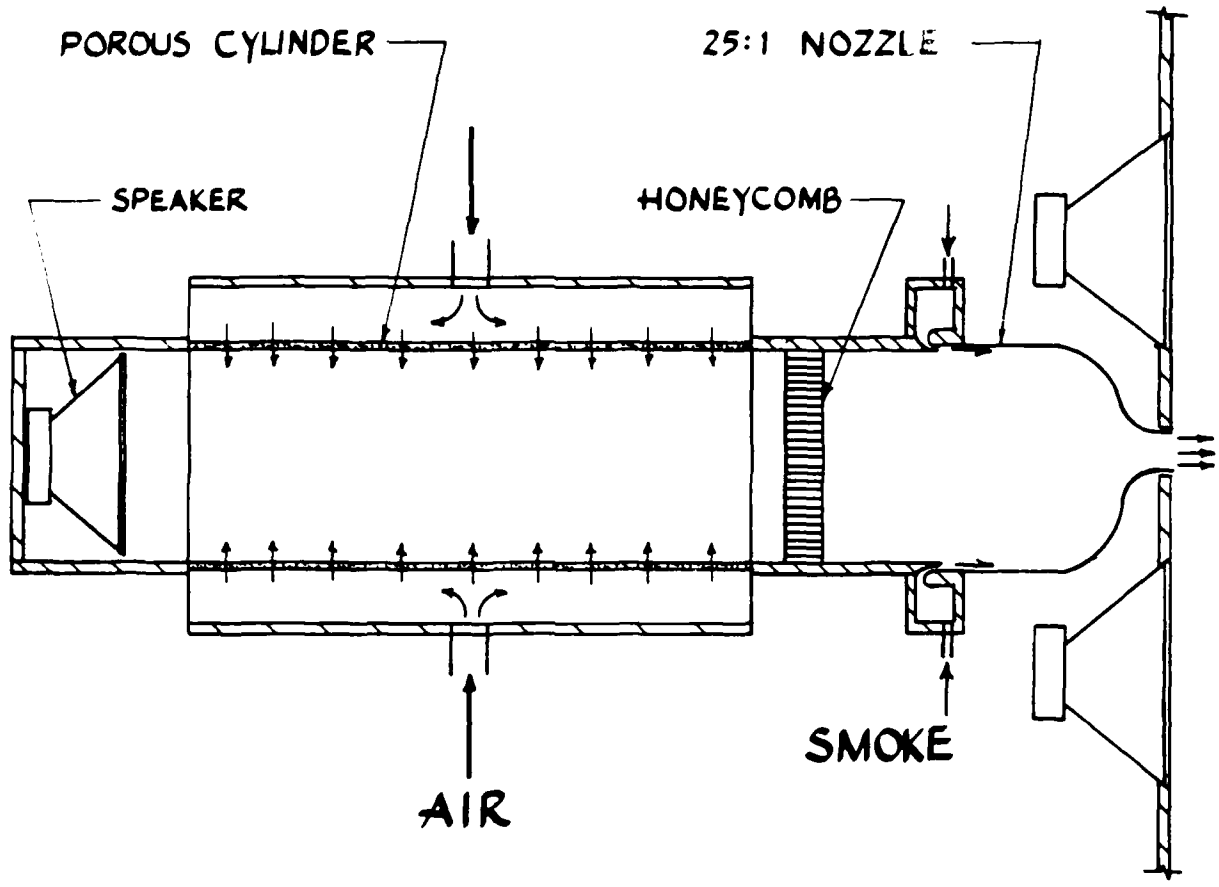

Figure 1. Schematic of jet facility.

Figure 2. Natural jet at Re = 10,000.

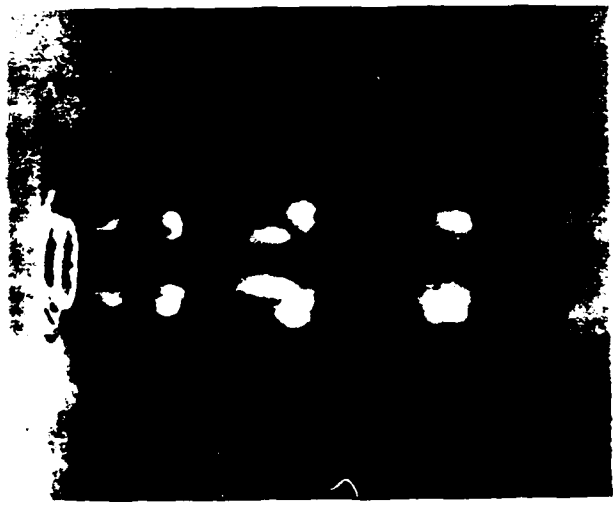

Figure 3. Axially-excited jet. Re = 10,000, St = 0.60, f_a = 192 Hz, and A_a = 0.03%.

Figure 4. Cross-section of axially-excited jet. Re = 20,000, St = 0.60, f_a = 386 Hz, and A_a = 0.03%.

Figure 6. Cross-section of bifurcating jet. Re = 10,000, St = 0.55, f_a = 180 Hz, f_t = 90 Hz, A_a = 0.12%, and A_t = 0.04%.

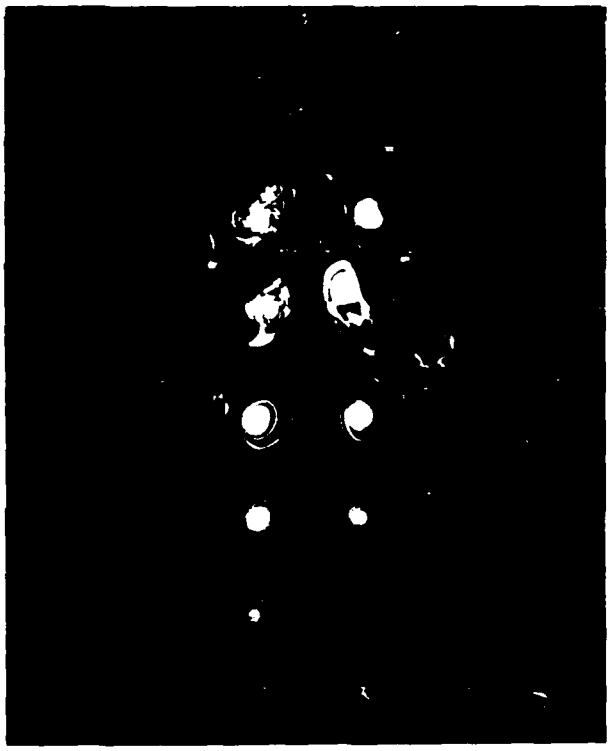

Figure 5. Cross-section of axially-excited jet. Re = 10,000, St = 0.55, f_a = 180 Hz, and A_a = 0.12%.

Figure 7. Cross-section of bifurcating jet. Re = 20,000, St = 0.60, f_a = 386 Hz, f_t = 193 Hz, A_a = 0.03%, and A_t = 0.03%.

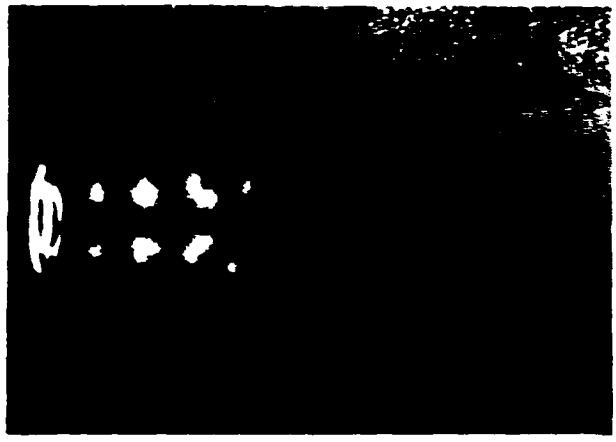

(a)

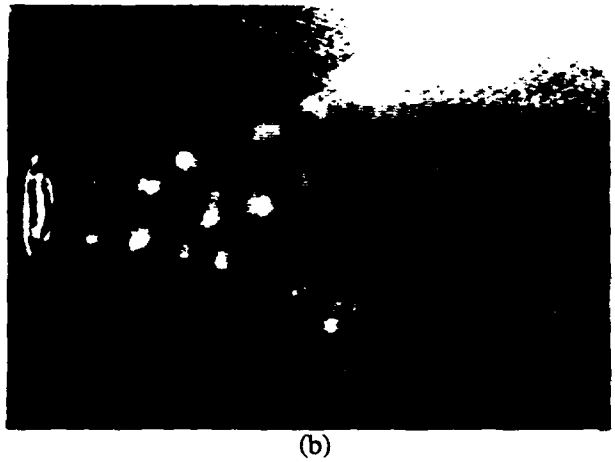

(b)

(c)

Figure 8. Video images of bifurcating jets at different transverse excitation amplitudes.
Re = 10,000, St = 0.60, f_a = 192 Hz,
f_t = 96 Hz, and A_a = 0.05%.
(a) A_t = 0.01%, (b) A_t = 0.02%, (c) A_t = 0.04%.

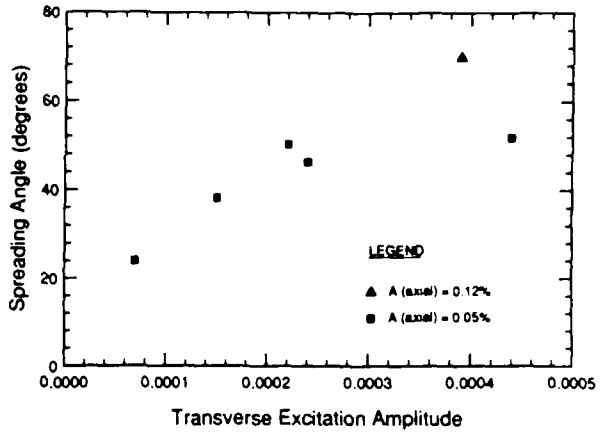

Figure 9. Variation of spreading angle with excitation amplitude.

Bifurcating Air Jets at Higher Subsonic Speeds

D. E. Parekh and W. C. Reynolds
Stanford University
Stanford, CA

SIXTH SYMPOSIUM
ON TURBULENT SHEAR FLOWS
September 7-9, 1987
Toulouse, France

BIFURCATING AIR JETS AT HIGHER SUBSONIC SPEEDS

D. E. Parekh and W. C. Reynolds
Stanford University

ABSTRACT

Dual-mode, dual-frequency acoustic excitation of round air jets is described. The jet evolution and structure is documented by flow visualization at velocities up to 75 m/s and Reynolds numbers to 100,000. The ratio of the axial to helical excitation frequencies is exactly two. This type of forcing causes the jet to spread dramatically in one plane. The spreading angle increases with excitation amplitude to angles as high as 70 degrees.

INTRODUCTION

The sensitivity of jets to sound has fascinated researchers for many decades. Brown demonstrated that laminar jets develop vortex structures and increase in spreading angle in response to acoustic excitation at various critical frequencies (1). Most current work focuses on jets consisting of an axisymmetric shear layer and a potential core. In this case the shear layer rolls up to form distinct vortex rings unlike the laminar jets of Brown which form vortex structures comprised of the entire jet stream.

The vortex-formation frequency can be fixed by axial excitation. This single-mode forcing can control jet growth by enhancing or suppressing vortex pairing (2,3). The "collective interaction" of several vortices due to subharmonic forcing has been demonstrated in mixing layers (4). This type of forcing has also been applied to high speed jets (5) and jets issuing from asymmetric nozzles (6).

The study of excited jets has involved multiple-frequencies and multiple-modes. A study of active cancellation of pure tones in jets involved simultaneous perturbations at two frequencies (7). Other work has focused on the changes in initial shear layer development in response to multiple-frequency forcing (8).

Properly combining axial and first-order helical modes can dramatically alter the structure and momentum transport of round jets. This type of *dual-mode* forcing can cause a jet to split into two distinct streams when the ratio of the axial to helical frequency is two. These phenomena occur only within a small range of Strouhal numbers, and within that range the spreading angle increases with St. These dramatic changes in jet development were discovered in a study of mechanically-perturbed round water jets at a Reynolds number of 4,000 (9). Similar jet development was observed in acoustically-excited air jets in the Reynolds number range of 10,000 to 20,000 (10).

This work extends the study of bifurcating air jets to Re of 100,000. Since the apparatus described in Ref. 10 is inadequate to produce the high levels of excitation required at higher velocities, a new acoustic excitation system was developed. The response of the jet at various Reynolds numbers is visually documented.

EXPERIMENTAL APPARATUS AND APPROACH

Flow System

The experimental apparatus is shown schematically in Fig. 1. Air flows through a porous bronze cylinder into the plenum and out through a 2-cm-diameter nozzle. The two-piece nozzle has a carefully machined fifth-order polynomial profile with zero slope at inlet and exit. The transition from the lower to the upper half of the nozzle occurs at the inflection point of the profile. The area contraction ratio is 25 to 1, and the length-to-diameter ratio is 5.

The jet exit is positioned in the center of a 60 cm x 60 cm flat panel and is flush with this panel. Baffles made of particle board and Sonex acoustical foam surround the jet on all four sides. These baffles are located 1 m from the jet on each side. The fume hood located 1.3 m above the jet is lined with Sonex foam. Entrained air flows into the test cell through the 0.8-m gap between the baffles and the floor.

Flow Visualization

A small 0.5-mm annular gap between the two halves of the nozzle provides a passage for injecting a fluid marker into the boundary layer. In these

in smoke reaching the jet centerline about one diameter closer to the jet exit (Fig. 8).

An axially-excited jet at Re of 100,000 is shown in Fig. 9. The high level of forcing causes the shear layer to turn turbulent at the exit. At low levels of excitation (below 120 dB), the shear layer remains laminar for the same distance as in the unforced jet (Fig. 6). As previously discovered (10), the spreading angle increases with excitation amplitude to angles as high as 70 degrees (Figs. 10 and 11). At the lower Reynolds numbers, increasing the helical excitation amplitude beyond a certain level does not increase the spreading angle and in some instances seems to reduce it. This is true regardless of how the axial excitation is introduced. The excitation levels required to reach this saturation level is found to increase with Reynolds numbers.

Adjusting the phase between the axial and helical signals rotates the plane in which the jet bifurcates. By rotating the jet such that it bifurcates in the plane perpendicular to the light sheet, one obtains the image in Fig. 12. Since the jet fluid moves away from this bisecting plane, the smoke density along the jet centerline decreases rapidly. The striking difference between the cross-sections in Figs. 10 and 11 demonstrates the fact that the bifurcating jet spreads rapidly in one plane rather than axisymmetrically.

CONCLUSIONS

The effect of combined axial and helical excitations on the development of round, turbulent air jets has been studied by flow visualization. Setting the axial frequency at exactly double the helical frequency causes the jet to spread rapidly in one diametrical plane. Increasing the amplitude of the helical excitation results in spreading angles as high as 70 degrees. However, increases above a certain level do not further amplify the spreading angle. Higher levels of excitation are required to reach this saturation level at higher Reynolds numbers. This work demonstrates that dual-mode forcing can cause jets to bifurcate at velocities up to 75 m/s and Reynolds numbers up to 100,000.

ACKNOWLEDGMENTS

This work was sponsored by the Air Force Office of Scientific Research under Contract AF-F49620-86-K-0020. The authors wish to thank Mr. Philippe Juvet for his assistance in the laboratory and in the preparation of this paper.

REFERENCES

1. Brown, G. B., "On Vortex Motion in Gaseous Jets and the Origin of Their Sensitivity to Sound," Proc. Phys. Soc., vol. 47, pp. 703-732 (1935).
2. Bouchard, E. E., and W. C. Reynolds, "The Effects of Forcing on the Mixing-Layer Region of a Round Jet," Unsteady Turbulent Shear Flows, IUTAM Sym., pp.370-379 (1981).
3. Zaman, K. B. M. Q., and A. K. M. F. Hussain, "Vortex Pairing in a Circular Jet Under Controlled Excitation," J. Fluid Mech., pp. 449-491 (1980).
4. Ho, C. M., and L. S. Huang, "Subharmonics and vortex merging in mixing layers," J. Fluid Mech., pp. 443-473 (1982).
5. Lepicovsky, J., K. K. Ahuja, W. H. Brown, and P. J. Morris, "Acoustic Control of Free Jet Mixing", AIAA paper 85-0569 (1985).
6. Kibens, V., and R. W. Wlezien, "Active Control of Jets from Indeterminate-Origin Nozzles," AIAA paper 85-0542 (1985).
7. Arbey, H., and J. E. Ffowcs Williams, "Active Cancellation of Pure Tones in an Excited Jet," J. Fluid Mech., pp. 445-454, (1984).
8. Ng, T. T. and T. A. Bradley, "Effect of Multi-Frequency Forcing on the Near Field Development of a Jet," AIAA paper 87-0054 (1987).
9. Lee, Mario, and W. C. Reynolds, "Bifurcating and Blooming Jets," Fifth Symposium on Turbulent Shear Flows, pp. 1.7-1.12 (1985).
10. Parekh, D. E., W. C. Reynolds, and M. G. Mungal, "Bifurcation of Round Air Jets by Dual-Mode Acoustic Excitation," AIAA paper 87-0164 (1987).

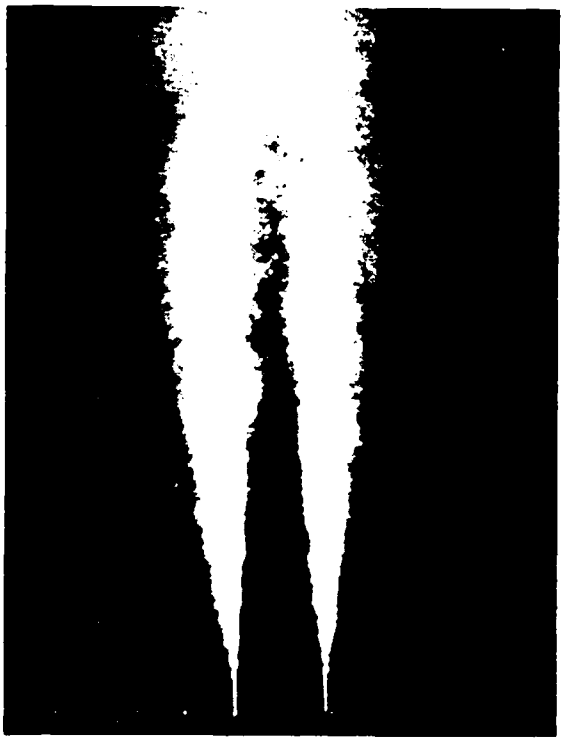

Figure 5. Natural jet at Re = 50,000 (N = 32).

Figure 7. Axially-excited jet at Re = 50,000 (N = 32)

Figure 4. Natural jet at Re = 200,000 (N = x

Figure 8. Bifurcating jet at Re = 50,000, N = 32, H = 3/4 3B

Figure 9. Axially-excited jet at Re = 100,000 (N = 8). A = 130 dB.

Figure 11. Bifurcating jet at Re = 100,000 (N = 8). A = 130 dB and H = 124 dB.

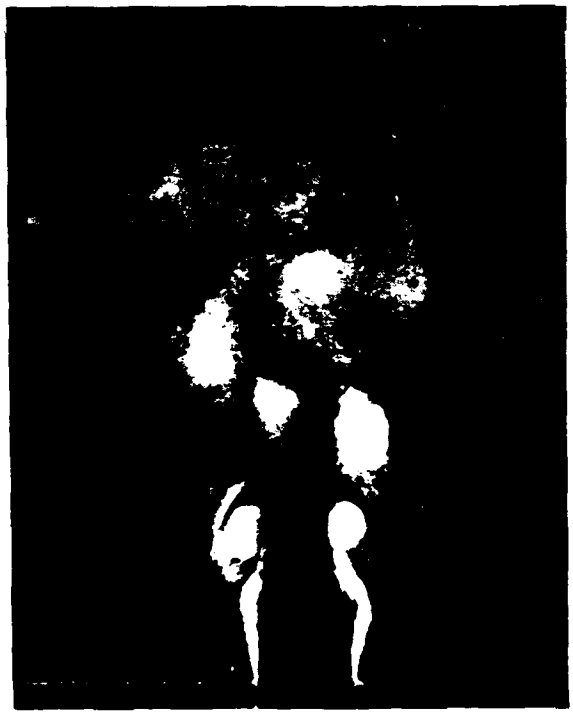

Figure 10 Bifurcating jet at Re = 100,000 (N = 8). A = 130 dB and H = 118 dB.

Figure 12 Bifurcating jet at Re = 100,000 (N = 8). Bisecting-plane view. A = 130 dB and H = 118 dB.

ERRATA

1. Page 3: "Figs. 10 and 11 demonstrates" should be "Figs. 10 and *12* demonstrates."

2. Page 4: "Figure 4. . . . (N = 32)" should be "Figure 4. . . . (N = *8*)."

END

DATE

FILMED

3-88

DTIC